The OsABCI7 Transporter Interacts with OsHCF222 to Stabilize the Thylakoid Membrane in Rice[1][OPEN]

Yan He, Yongfeng Shi, Xiaobo Zhang, Xia Xu, Huimei Wang, Liangjian Li, Zhihong Zhang, Huihui Shang, Zhonghao Wang, and Jian-Li Wu[2,3]

State Key Laboratory of Rice Biology, China National Rice Research Institute, Chinese Academy of Agricultural Sciences, Hangzhou 310006, China

ORCID IDs: 0000-0002-2769-6285 (X.X.); 0000-0003-3480-1503 (J.-L.W.)

The thylakoid membrane is a highly complex membrane system in plants and plays crucial roles in the biogenesis of the photosynthetic apparatus and plant development. However, the genetic factors involved in chloroplast development and its relationship with intracellular metabolites are largely unknown. Here, a rice (*Oryza sativa*) *chlorotic and necrotic leaf1* (*cnl1*) mutant was identified and map-based cloning revealed that a single base substitution followed by a 6-bp deletion in the *ATP-binding cassette transporter I family member7* (*OsABCI7*) resulted in chlorotic and necrotic leaves with thylakoid membrane degradation, chlorophyll breakdown, photosynthesis impairment, and cell death in *cnl1*. Furthermore, the expression of *OsABCI7* was inducible under lower temperatures, which severely affected *cnl1* chloroplast development, and etiolated *cnl1* seedlings were unable to recover to a normal green state under light conditions. Functional complementation and overexpression showed that *OsABCI7* could rescue the *cnl1* chlorotic and necrotic phenotype. OsABCI7 interacted with HIGH CHLOROPHYLL FLUORESCENCE222 (OsHCF222) to regulate cellular reactive oxygen species (ROS) homeostasis for thylakoid membrane stability. OsABCI7 localized to thylakoid membranes, while OsHCF222 targeted to endoplasmic reticulum and chloroplasts. Exogenous application of ascorbic acid eased the yellowish leaf phenotype by increasing chlorophyll content and alleviating ROS stress in *cnl1*. Unlike *cnl1*, the CRISPR/Cas9-mediated *OsHCF222* knockout lines showed chlorotic leaves but were seedling lethal. Our results provide insight into the functions of ABC transporters in rice, especially within the relationship between ROS homeostasis and stability of thylakoid membranes.

In plant leaves, mature chloroplasts develop from proplastids, a type of colorless and small precursor, with surrounded inner and outer envelopes and rudimentary inner membranes. These rudimentary membranes elaborate into an inerratic thylakoid membrane system during leaf development. As the photosynthetic machinery, the thylakoid membrane complex is composed of four major protein complexes: PSII, cytochrome b_6f (Cytb6f), PSI, and ATP synthase. Thylakoid membrane biogenesis is involved in a variety of processes, such as gene transcriptional regulation, post-translational regulation and modification, and protein complex assembly (Lyska et al., 2013). In chloroplasts, the thylakoid membrane is regularly stacked to increase the membrane area for a higher photosynthetic efficiency, and a well-developed thylakoid membrane system is also closely associated with chloroplast development (Kobayashi et al., 2007). To date, many genes exhibiting crucial regulatory roles in chloroplast development under low temperatures have been identified (Wang et al., 2016; Sun et al., 2017; Liu et al., 2018; Cui et al., 2019), while genetic factors affecting the relationship between chloroplast development and intracellular metabolites are largely unknown.

Endogenous reactive oxygen species (ROS) are mainly produced at the PSI and PSII reaction centers in thylakoids. Usually, an oxygen molecule obtains an electron and is reduced to a superoxide anion (O_2^-), and its disproportionation by a superoxide dismutase (SOD) produces hydrogen peroxide (H_2O_2; Asada et al., 1974). To protect chloroplasts from the direct damage by H_2O_2, the newly produced thylakoidal H_2O_2 is promptly scavenged; hence, H_2O_2 is not accumulated in intact chloroplasts (Asada, 2006). In this process, H_2O_2 is reduced into water by ascorbate acid (AsA) catalyzed by the plant- and algae-specific H_2O_2-scavenging enzyme, ascorbate peroxidase (APX; Asada, 1992). Additionally, catalase (CAT) can directly reduce H_2O_2 into water. Once the balance of ROS production and scavenging is broken, oxidative damage induced by ROS preferentially occurs in chloroplast thylakoids, leading to chlorophyll degradation as well as DNA damage (Ahmad

[1]This work was supported by the Ministry of Science and Technology of China (grant no. 2016YFD0101104) and the State Key Laboratory of Rice Biology.

[2]Author for contact: beishangd@163.com.

[3]Senior author.

The author responsible for distribution of materials integral to the findings presented in this article in accordance with the policy described in the Instructions for Authors (www.plantphysiol.org) is: Jian-Li Wu (beishangd@163.com).

Y.H. and J.-L.W. designed the experiments; Y.H., Y.S., X.Z., X.X., H.W., L.L., Z.Z., H.S., and Z.W. performed the experiments; Y.H. analyzed the data; Y.H. and J.-L.W. wrote the manuscript; J.-L.W. supervised the study.

[OPEN]Articles can be viewed without a subscription.

www.plantphysiol.org/cgi/doi/10.1104/pp.20.00445

et al., 2010; Gill and Tuteja, 2010; Soares et al., 2016). Besides biotic and/or abiotic stresses, mutations of relevant genes are important causes for inducing ROS bursts, resulting in various morphological variations, such as premature senescence, yellowing, and spotted leaves (Huang et al., 2016; Xu et al., 2018; Sathe et al., 2019; Wang et al., 2019).

The ATP-binding cassette (ABC) transporter is an ancient and large protein superfamily consisting of eight major subgroups (ABCA–ABCH). In plants, the members of the ABCA to ABCG subgroups are widely distributed, while the ABCH members are absent (Garcia et al., 2004). ABC proteins, with six conserved typical motifs, including ABC signature, Walker-A, Walker-B, D-loop, H-loop, and Q-loop sequence, are well known for their functions in intracellular/extracellular substrate transporting (Huang et al., 2009). Not only limited to the transport of ions, lipids, monosaccharides, hormone secondary metabolites, and xenobiotics, recent studies have demonstrated that ABC proteins are also involved in plant defense response, pathogen resistance, and male reproduction (Matsuda et al., 2012; Zhao et al., 2015; Garroum et al., 2016). Plants share the specific bacterial-type ABC transporters with prokaryotes, designed as ABCI subgroup. In Arabidopsis (*Arabidopsis thaliana*), both chloroplast-localized AtABCI10 and AtABCI11 (AtNAP14) proteins participate in the regulation of chloroplast metal homeostasis, and their corresponding transfer DNA mutants are totally devoid of chlorophylls with severely deformed leaf structures, aberrant chloroplasts, and defective photosynthetic capacity (Shimoni-Shor et al., 2010; Voith von Voithenberg et al., 2019). In rice (*Oryza sativa*), OsABCI8 is indispensable for chloroplast development by engaging iron transportation and homeostasis (Zeng et al., 2017). OsABCI12 (STAR2) interacts with STAR1 to form a complex responsible for the transport of UDP-Glc and detoxification of aluminum (Huang et al., 2009).

The rice high-chlorophyll-fluorescence (*hcf*) mutants are unable to utilize absorbed light efficiently (Meurer et al., 1996). Due to lack of photosynthetic autotrophy, most *hcf* mutants are seedling lethal yet able to survive on Suc-supplemented medium (Schult et al., 2007; Link et al., 2012; Hartings et al., 2017). Here, we isolated an ABC transporter I family member7 (OsABCI7), which interacts with HIGH CHLOROPHYLL FLUORESCENCE222 (OsHCF222) to maintain thylakoid membrane stability via regulating ROS homeostasis in rice.

RESULTS

cnl1 Is Defective in Plant Growth and Development

The *chlorotic and necrotic leaf1* (*cnl1*) mutant was isolated from an ethyl methylsulfonate-induced indica rice var. Zhongjian 100 (wild type) mutant bank. Under natural field conditions, *cnl1* exhibited chlorotic and necrotic phenotypes on older leaves with the vestigial thylakoid membrane ultrastructure and lower levels of chlorophyll contents ~40 d after sowing (Fig. 1, A–D; Supplemental Fig. S1, A–C). Due to abnormal chlorophyll degradation, *cnl1* showed significantly compromised net photosynthesis rate, higher intercellular CO_2 concentration, and transpiration rate compared with wild type (Supplemental Fig. S1, D–G).

In addition, *cnl1* also exhibited a poorer performance in major agronomic traits compared with wild type (Fig. 1, E–I). The II and III internode lengths were remarkably decreased in *cnl1* compared to wild type at the heading stage (Fig. 1, J and K), and microscope observation directly revealed that the shorter stature of *cnl1* resulted from the reduced length of cells in the stems (Fig. 1, L–N). These results indicated that the *cnl1* mutation resulted in multiple deficiencies in plant growth and development.

CNL1 Encodes Rice ABC Transporter I Family Member7 (OsABCI7)

To determine the genetic control of the *cnl1* phenotype, we crossed *cnl1* with two wild type japonica rice cultivars (cv ReYan 1 and cv ORO, respectively). As shown in Table 1, the wild-type F_1 plants and expected mendelian 3:1 (wild type:mutant) ratios in F_2 populations indicated monogenic and recessive genetic control of the mutant trait.

We selected 755 F2 mutant-type individuals derived from the cross *cnl1* × cv ReYan 1 to map the mutation. The *OsABCI7* locus preliminarily mapped to the long arm of chromosome 11 between the markers RM287 and RM229, and we narrowed the location to a 116-kb region containing 12 open reading frames (ORFs; Fig. 2A; Supplemental Table S1). Sequencing of these 12 ORFs revealed a single nucleotide substitution (C to A) followed by a 6-bp deletion at the junction of exon 8 and intron 8 of *LOC_Os11g29850*, resulting in a 17-bp alternative splicing deletion at the end of exon 8, which finally led to a frame shift and premature stop codon (Fig. 2B; Supplemental Figs. S2 and S3A). According to the Rice Annotation Project Database (https://rapdb.dna.affrc.go.jp/), *LOC_Os11g29850* belongs to the ABC transport superfamily ABCI subgroup member 7 (referred to *OsABCI7*). The structural changes of OsABCI7 were intuitively visible by modeling the three-dimensional structures of wild-type (OsABCI7) and mutant (ΔOsABCI7) proteins (Supplemental Fig. S3B). Additionally, the derived cleaved amplified polymorphic sequence analysis was performed to confirm the mutation in the genomic DNA, and the agarose electrophoresis verified the presence of the 17-bp deletion in the cDNA of Δ*OsABCI7* (Fig. 2, C and D). *OsABCI7* encodes an ABC transport protein and contains all typical conserved motifs of ABC transporters, namely, the Walker-A, Q-loop, ABC signature, Walker-B, D-loop, and H-loop motifs (Supplemental Fig. S2).

To confirm whether the mutation was responsible for the *cnl1* phenotype, we performed a complementation

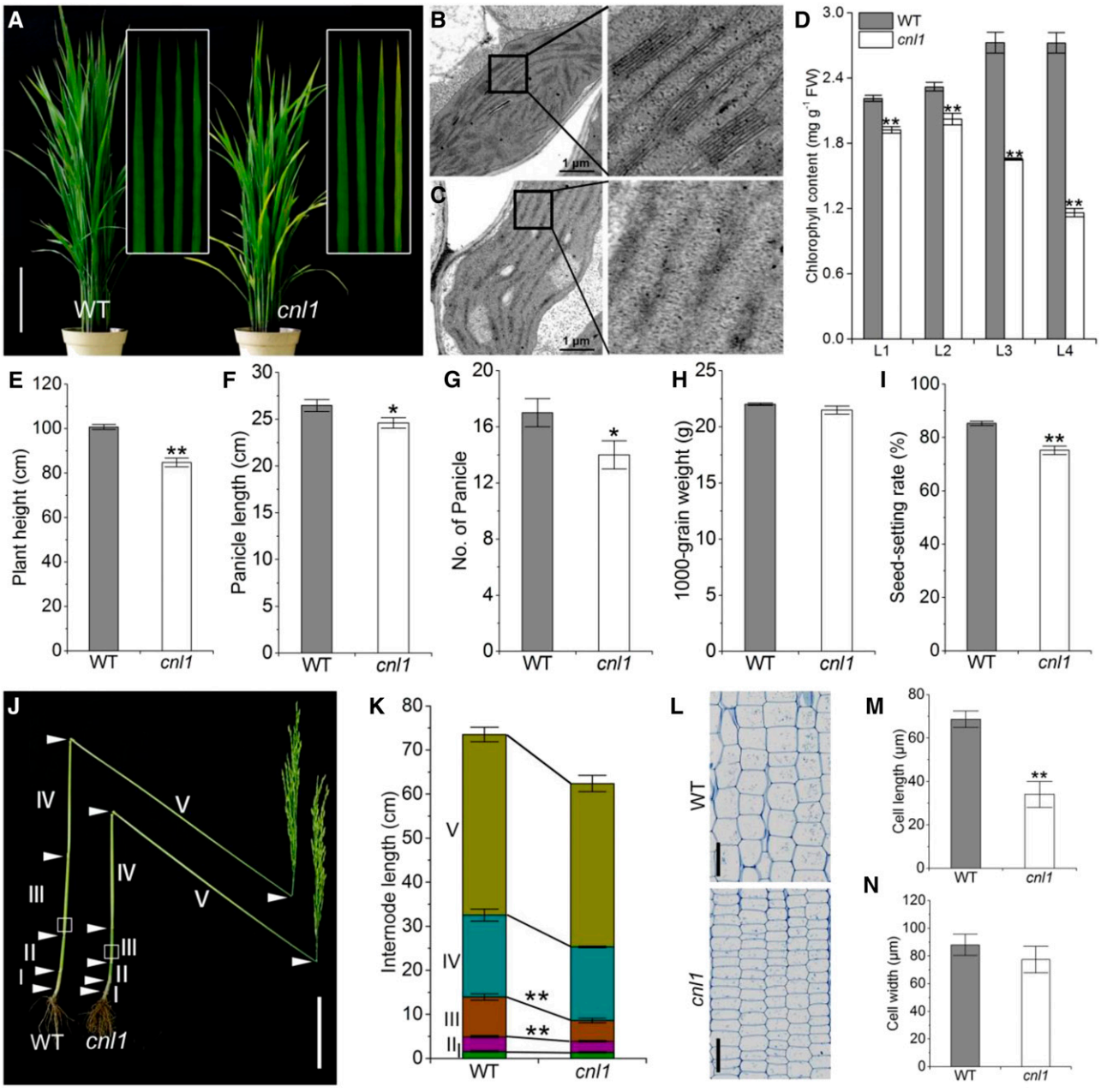

Figure 1. Phenotypic characterization of *cnl1*. A, Wild-type (WT) and *cnl1* at the tillering stage (45 d after field transplanting). Insets show magnified views of the four leaves (L1–L4) from top to bottom of wild type and *cnl1*. Bar = 20 cm. B and C, Chloroplast ultrastructure in mesophyll cells of L4 in wild type (B) and *cnl1* (C) in A. D, Chlorophyll contents in different leaves of wild type and *cnl1*. L1 to L4 represent the four leaves shown in A (from left to right), respectively. E to I, Major agronomic traits of wild type and *cnl1*. J, Comparison of main stems from wild type and *cnl1*. Arrows indicate the node positions. Bar = 10 cm. K, Internode lengths of main stems in wild type and *cnl1* at the mature stage. L, Longitudinal sections of the corresponding parts of internode III from wild type and *cnl1* as marked by the white boxes in J. Bars = 100 μm. M and N, Comparison of cell length (M) and cell width (N) of internode III in wild type and *cnl1*. Data are means ± SD ($n = 5$). Asterisks indicate significant difference by Student's *t* test (**$P < 0.01$ and *$P < 0.05$).

test by introducing 5.9-kb genomic DNA containing the promoter and the full genomic coding region of *OsABCI7* into *cnl1*-derived calli. All 15 independent positive T_0 complementary lines showed the normal green phenotype, mimicking the wild type (Fig. 2E). We also overexpressed the coding sequence (CDS) of *OsABCI7* in *cnl1* using the vector pCAMBIA1300-UBI (Zhang et al., 2018), which confers maize (*Zea mays*) *Ubiquitin1* promoter and the coding region for an N-terminal hemagglutinin (HA) epitope tag to the

Table 1. *Genetic control of the* cnl1 *phenotype*

Cross	F_1	No. F2 Individuals		χ^2 (3:1)
		Wild Type	Mutant Type	
cnl1 × wild type	Wild type	127	34	1.29
cnl1 × cv ReYan 1	Wild type	923	283	1.51
cnl1 × cv ORO	Wild type	399	112	2.59

CDS (Supplemental Fig. S4, A and B), and the mutant phenotype was rescued in all 24 T_0 positive overexpression lines (Fig. 2E). These results demonstrated that Δ*OsABCI7* was responsible for the *cnl1* phenotype, and the CDS of *OsABCI7* encoded a functional protein. Compared with wild type, the expression of *OsABCI7* was significantly downregulated in *cnl1* but recovered to wild-type levels in complementary plants, and the expression level of *OsABCI7* in overexpression plants was upregulated by about 6-fold in wild type (Fig. 2F). To investigate whether the low expression of *OsABCI7* would lead to the *cnl1* phenotype, we also performed RNA interference analysis of *OsABCI7* and obtained 21 T_0 positive lines that exhibited significantly down-regulated *OsABCI7* expression with normal wild-type phenotype (Supplemental Fig. S4, D–H). We therefore concluded that the low *OsABCI7* expression was unable to cause *cnl1* phenotype, and the rescues of *cnl1* by complementation and overexpression were due to the recovered *OsABCI7* function and not the recovered *OsABCI7* expression. Furthermore, similar expression levels of *OsABCI7* were detected from the tip to the base of the yellowing flag leaves, indicating low relevance between *OsABCI7* expression and natural leaf yellowing (Supplemental Fig. S4C).

Leaf yellowing and senescence are largely accompanied with ROS accumulation (Buchanan-Wollaston et al., 2003). Thus, we first measured the levels of ROS, including H_2O_2 and O_2^-, and found that ROS were higher in *cnl1* compared with wild type (Fig. 2, G and H). We then detected the activities of ROS scavenging enzymes and the contents of malondialdehyde (MDA) and soluble proteins. The activities of APX and CAT, two key H_2O_2 scavenging enzymes, as well as soluble protein contents, were significantly lower in *cnl1* than in the wild type (Fig. 2, I and J; Supplemental Fig. S5A). In contrast, the level of MDA, an indicator of ROS-induced lipid peroxidation, was significantly higher in *cnl1* than in the wild type (Fig. 2L). Peroxidase activity was higher in *cnl1* compared with wild type, while SOD activity was similar between the two genotypes (Fig. 2K; Supplemental Fig. S5B). These results suggested that Δ*OsABCI7* disrupted the balance between ROS production and scavenging. Moreover, ROS accumulation in *cnl1* was also confirmed by nitrotetrazolium blue chloride and 3,3′-diaminobenzidine staining (Supplemental Fig. S6C). As expected, the ROS contents and ROS scavenging enzyme activities in the complementary and overexpression line recovered to wild-type levels (Fig. 2, G–L). In addition, chlorophyll fluorescence and chlorophyll levels in the complementary and overexpression lines also recovered to the wild-type levels (Supplemental Fig. S6, A and B; Supplemental Table S2). Taken together, our results demonstrated that both the normal expression and overexpression of *OsABCI7* in the *cnl1* background could fully rescue the physiological and biochemical defects of *cnl1*. Notably, in contrast to wild type, the overexpression plants exhibited prominently decreased H_2O_2 and O_2^- contents and increased APX activities (Fig. 2, G–I). We speculated that *OsABCI7* was involved in chloroplast-specific ROS scavenging since the H_2O_2 scavenging largely relies on APX in chloroplasts (Asada, 2006).

DNA Damage and DNA Damage Response Are Induced in *cnl1*

The programmed cell death (PCD) phenotype was detected in *cnl1* by trypan blue staining (Supplemental Fig. S6C). Since PCD associates with DNA breakdown, we conducted the terminal deoxyribonucleotidyl transferase-mediated dUTP nick-end labeling (TUNEL) assay to determine the nuclear DNA fragmentation in the flag leaves of wild type and *cnl1*. Expectedly, few TUNEL-positive signals were detected in wild type, yet numerous nuclei exhibited TUNEL-positive signals in *cnl1* (Supplemental Fig. S7). Furthermore, we performed comet assay (single cell gel electrophoresis assay), a simple and effective method for evaluating DNA damage in cells (Speit and Hartmann, 2006), to test DNA damage in wild type and *cnl1*. Consistent with the TUNEL assay, significantly increased DNA damage was found in *cnl1* compared with wild type (Fig. 3, A–C).

DNA repair and DNA replication occur in response to DNA damage. Indeed, eight up-regulated marker genes associated with DNA repair and replication were found in *cnl1* (Fig. 3D). *Poly (ADP-ribose) polymerase* (*PARP*), *ataxia telangiectasia mutated* (*ATM*), and *ATM-rad3-related* (*ATR*) are classified to the ATM/ATR-mediated signaling response (Zhou and Elledge, 2000; Culligan et al., 2006). *DNA repair protein Rad51* (*RAD51A2* and *RAD51C*) belong to the RecA/Rad1 protein family, which is required for the homologous recombination repair pathway (Durrant et al., 2007). *RNRL1* and *RNRS1* encode the large and small subunits of ribonucleotide reductase (RNR), respectively, regulating the deoxyribonucleotide production rate for DNA synthesis and repair (Yoo et al., 2009). *RNA-dependent RNA polymerase6* (*RDR6*) acts in the biogenesis of multiple small RNAs (Song et al., 2012). In conclusion, Δ*OsABCI7* induced PCD and severe DNA

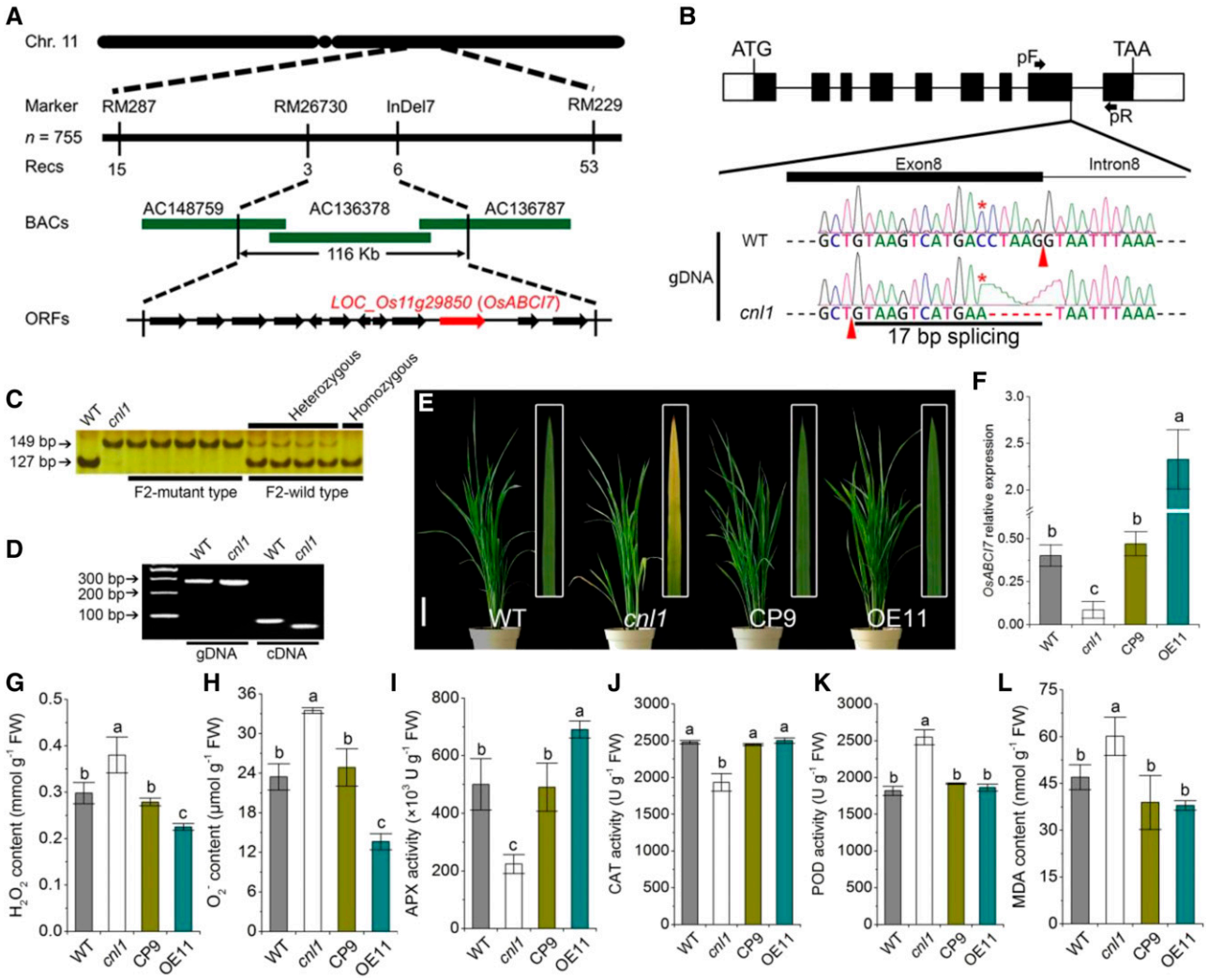

Figure 2. Map-based cloning of *OsABCI7* and ROS detection in *cnl1*. A, Mapping of the *OsABCI7* locus. The molecular markers and recombinant numbers are displayed. The candidate gene *OsABCI7*/*LOC_Os11g29850* is depicted in red. B, *OsABCI7* allele structure in wild type (WT) and *cnl1*. The white boxes, black boxes, and black lines represent untranslated regions, exons, and introns, respectively. The red stars indicate the nucleotide substitution, and red arrowheads indicate the splicing site of intron 8 in wild type and *cnl1*. pF and pR indicate the forward and reverse primer sites in D. C, Derived cleaved amplified polymorphic sequence confirmation of the mutation. PCR products were digested by *Sal*I from wild type but not from *cnl1* and detected by 6% polyacrylamide gel. D, PCR analysis showing the 17-bp splicing deletion of the eighth exon. The smaller band of *cnl1* cDNA resulted from the 17-bp alternative upstream splicing deletion as indicated in B. gDNA, Genomic DNA. Agarose gel concentration was 3.5%. E, Phenotypes of complementary (CP) and overexpression (OE) lines at 40 d after sowing. Insets show magnified views of the bottom second leaves. Bar = 10 cm. F, Relative expression of *OsABCI7* in wild-type, *cnl1*, and transgenic plants. Rice *UBIQUITIN* was used as an internal control. Data are means ± SD ($n = 3$). G to K, ROS levels, ROS scavenging enzyme activities and MDA contents in flag leaves of wild-type, *cnl1*, and transgenic plants at the heading stage. H_2O_2 content (G), O_2^- content (H), APX activity (I), CAT activity (J), peroxidase (POD) activity (K), and MDA content (L). Data are means ± SD ($n = 3$). Different letters indicate significant differences by one-way ANOVA and Duncan's test ($P < 0.05$).

damage and up-regulated expression of marker genes associated with DNA repair and replication.

OsABCI7 Is Constitutively Expressed and OsABCI7 Localizes to the Thylakoid Membrane

To validate if OsABCI7 localized to chloroplasts as predicted by TargetP 1.1 Server (http://www.cbs.dtu.dk/services/TargetP/), we fused the full CDS of *OsABCI7* to the N terminus of GFP driven by the CaMV35S promoter and transiently expressed the construct in rice protoplasts. The OsABCI7-GFP fusion protein indeed localized to chloroplasts (Fig. 4A). Notably, the ΔOsABCI7-GFP fusion protein also localized to chloroplasts, indicating the mutation of OsABCI7 did not change its chloroplast localization (Fig. 4A). Additionally, we truncated constructs to analyze the chloroplast transit peptide, and nearly all

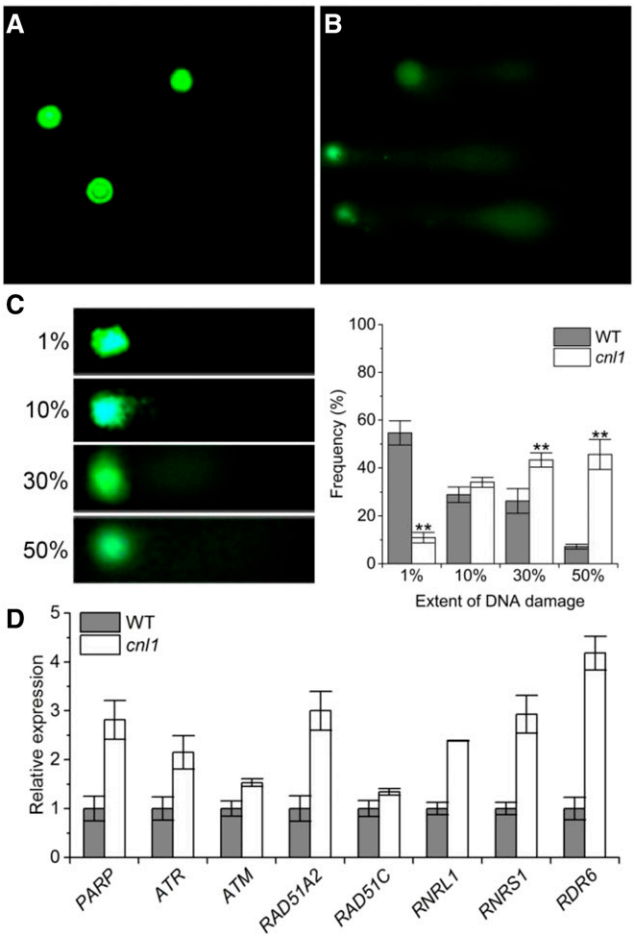

Figure 3. DNA damage detection and transcriptional level analysis of DNA damage repair- and replication-associated genes. A and B, Typical comets for DNA damage in nuclei of flag leaves from wild type (WT; A) and *cnl1* (B) at the heading stage. C, Four types of DNA damage extents in each nucleus are indicated by the units 1%, 10%, 30%, or 50%. An increased unit associated with a larger comet tail. Frequency distribution of four types of DNA damage extents in wild type and *cnl1*. Data are means ± SD ($n = 3$). Asterisks indicate significant difference by Student's *t* test (**$P < 0.01$). D, Transcriptional level analysis of DNA repair- and replication-associated genes by RT-qPCR. Rice *Ubiquitin* was used as an internal control. Data are means ± SD ($n = 3$).

fusion constructs with varying lengths of OsABCI7, such as OsABCI7$^{1–30aa}$, apparently localized to the chloroplast except for OsABCI7$^{30–276aa}$ and OsABCI7$^{50–276aa}$ (Fig. 4A). These demonstrated that the OsABCI7$^{1–30aa}$ may contain a chloroplast transit peptide indispensable for OsABCI7 chloroplast targeting. To detect the precise localization of OsABCI7, we performed immunoblot analysis using total proteins, chloroplasts, thylakoid fractions, and stromal fractions extracted from *OsABCI7* overexpression plants. A 32-kD protein was absent in stromal fractions while present in total proteins, chloroplasts, and thylakoid membrane fractions, confirming the thylakoid membrane localization of OsABCI7 (Fig. 4B).

We then detected *OsABCI7* expression levels in different organs using reverse transcription quantitative PCR (RT-qPCR). *OsABCI7* was expressed in all organs at different growth stages (Fig. 4O). Consistent with the RT-qPCR results, *GUS* expression was detected in all organs of *OsABCI7*$_{Pro}$*::GUS* transgenic plants (Fig. 4, C–N), further supporting the constitutive expression of *OsABCI7*.

OsABCI7 Is Required for Chloroplast Development under Cold Stress and Light-Dependent Chlorophyll Synthesis

Chloroplast development and chlorophyll synthesis are affected by light and temperature in rice (Wang et al., 2016; Sun et al., 2017; Wang et al., 2017). Wild type and *cnl1* were planted in a growth chamber under different temperature conditions. At 30°C, *cnl1* plants displayed a wild-type-like phenotype, though the chlorophyll content of *cnl1* was significantly lower than that of the wild type (Fig. 5A; Supplemental Fig. S8A). In contrast, *cnl1* showed pale green leaves at 25°C, and the pale green phenotype aggravated at 20°C with rapid decrease of chlorophyll contents compared with wild type (Fig. 5, B and C; Supplemental Fig. S8A). We then explored the kinetic expression of *OsABCI7* in wild type and *cnl1* under low-temperature treatment at 10°C, and *OsABCI7* expression increased rapidly by 2-fold after 2 h, by 2.5-fold after 4 h treatment, and recovered to the control level after 6 h of treatment (Fig. 5D), while *OsABCI7* expression increased 2- to 3-fold from 4 to 10 h treatment in *cnl1* (Supplemental Fig. S8B). The results indicated that *OsABCI7* transcription was induced by low temperature and likely acted as a signal factor responding to cold stress.

We also investigated the ultrastructure of chloroplasts in mesophyll cells of wild type and *cnl1* under different temperatures using transmission electron microscopy (TEM). At 30°C, intact chloroplast structure and well-formed grana thylakoids were observed in wild type and *cnl1* (Fig. 5E). In contrast, distinctly degraded chloroplasts and reduced grana thylakoids were found in *cnl1* at 25°C and 20°C compared with wild type (Fig. 5, F and G). These suggested that the developmental defects associated with the pale green phenotype in *cnl1* resulted from chloroplast breakdown induced by low temperatures. Furthermore, *OsABCI7* was essential for light-dependent chlorophyll synthesis during the greening of etiolated seedlings (Fig. 5, H–K), while *OsABCI7* transcription in wild type and *cnl1* was not relevant to the greening process (Fig. 5L). Collectively, the results suggested that *OsABCI7* was involved in light-dependent chlorophyll synthesis and required for chloroplast development under low temperature.

Thylakoid Membrane Complexes Are Impaired in *cnl1*

Thylakoid membrane biogenesis is regulated and assisted by many plastome- and nucleus-encoded genes, and thylakoid membrane protein complexes are composed of PSII, PSI, Cytb6f complex, and ATP

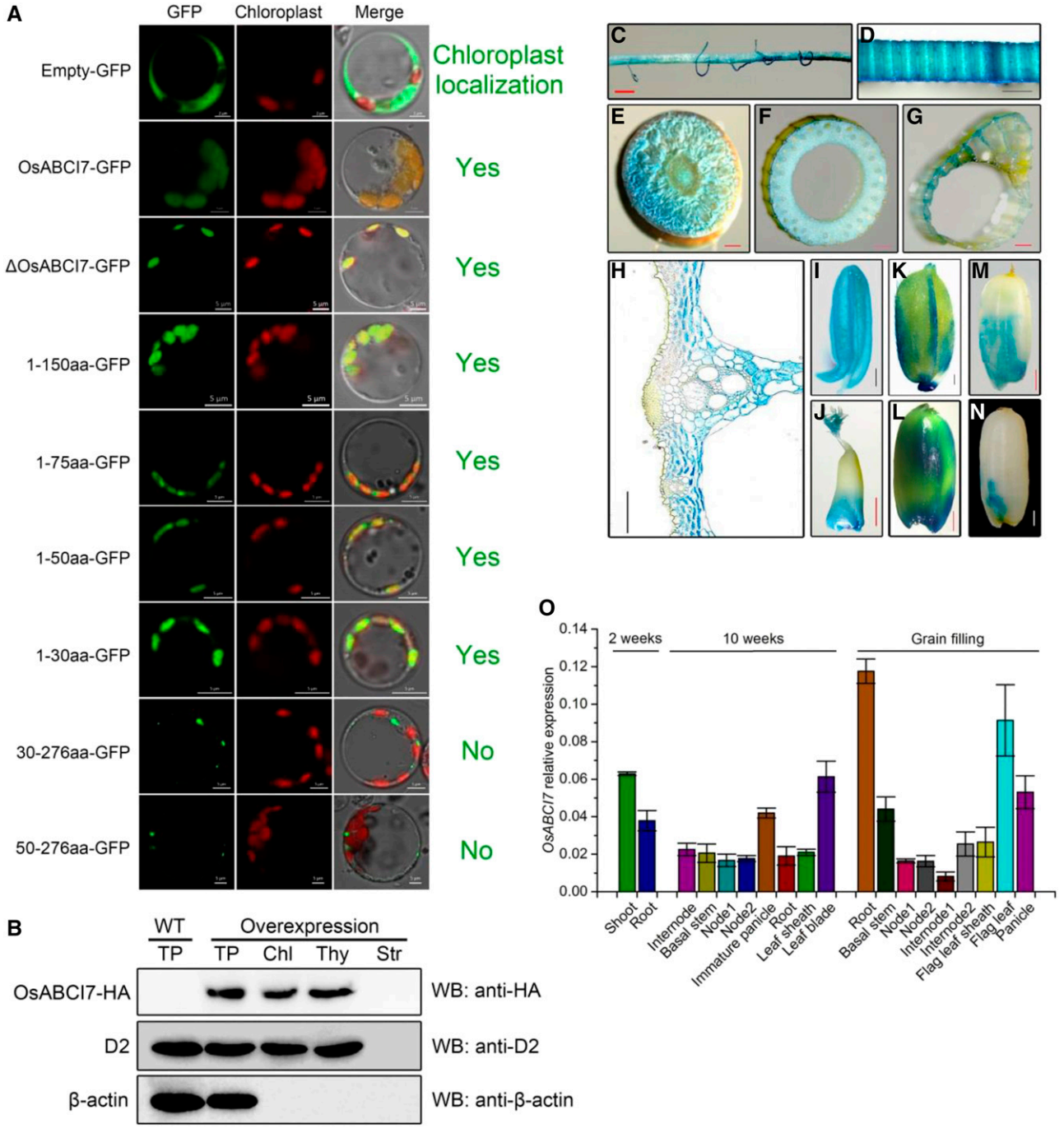

Figure 4. Subcellular localization and expression pattern of *OsABCI7*. A, GFP signals of different constructs in rice protoplasts. The full OsABCI7 protein contains 276 amino acids. ΔOsABCI7 represents the mutant OsABCI7 protein. Bars = 5 μm. B, Immunoblot analysis of OsABCI7. Protein samples were from *OsABCI7* (fused HA-tag) overexpression seedlings. Antiserum against HA-tag (anti-HA), D2 (thylakoid marker), and β-actin were used in blotting. TP, Total protein; Chl, chloroplast; Thy, thylakoid membrane fraction; Str, stroma fraction; WT, wild type. C to N, *GUS* staining of $OsABCI7_{Pro}$::*GUS* transgenic plants. Root (C), leaf blade (D), node V (E), culm (F), leaf sheath (G), leaf blade transverse slice (H), stamen (I), and seeds at different stages of development (J–N). Bars = 1 mm (B–F and H–M) and 100 μm (G). O, Relative expression of *OsABCI7* in various organs at different growth stages. Data are means ± SD (n = 3).

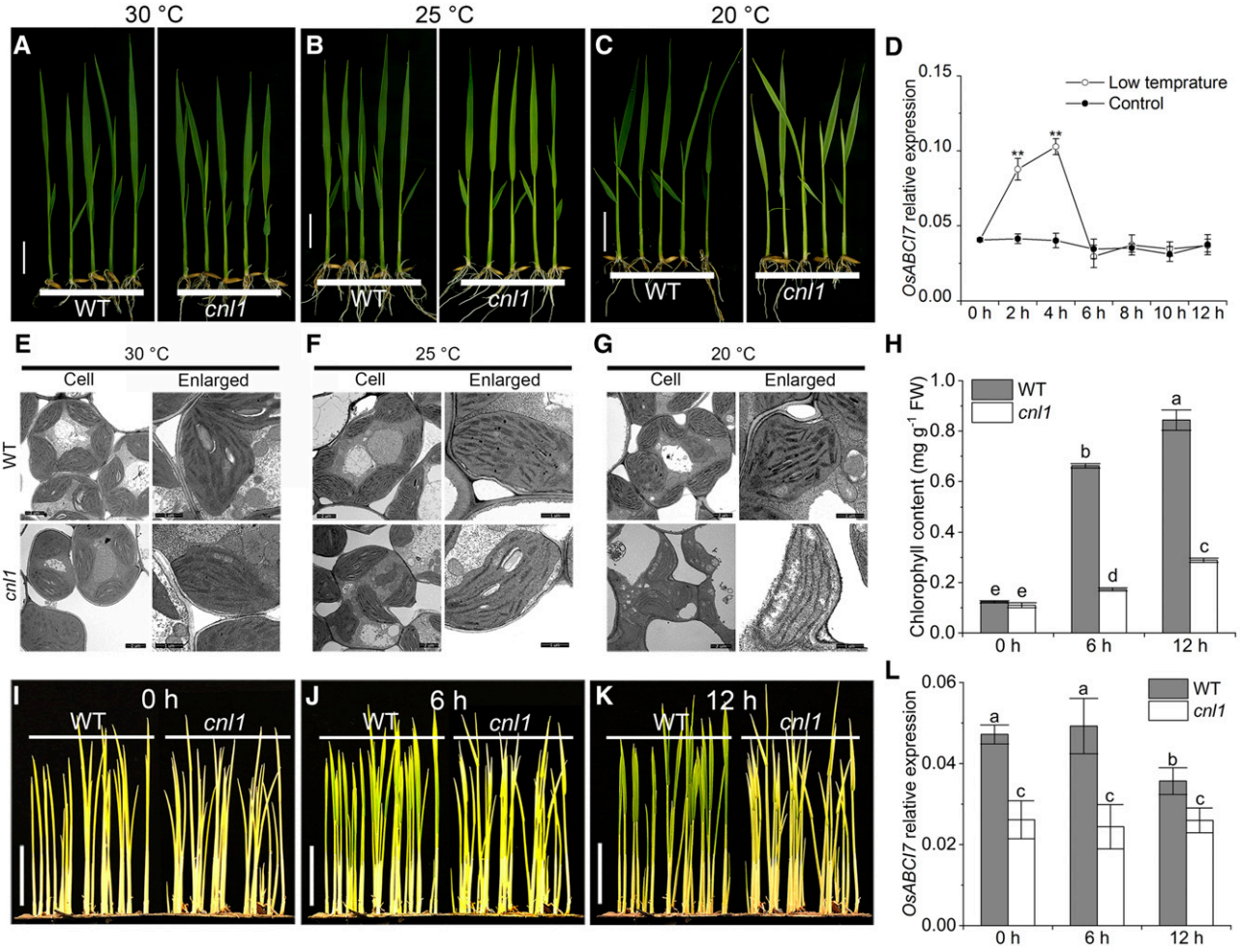

Figure 5. Phenotypic characterization of wild type (WT) and *cnl1* at different temperatures and light-dependent chlorophyll synthesis of wild type and *cnl1*. A to C, Phenotypic comparison of wild-type and *cnl1* seedlings at different temperatures. The wild type and *cnl1* were grown in growth chambers after germination for 10 d at 30°C (A) and 25°C (B) and 16 d at 20°C (C) with constant temperatures and 14 h light/10 h dark cycles (400 μmol m^{-2} s^{-1}). Bars = 2 cm. D, Kinetic analysis of *OsABCI7* expression in wild type at 10°C. Data are means ± SD ($n = 3$). Asterisks indicate significant difference by Student's *t* test (**$P < 0.01$). E to G, Ultrastructure of chloroplasts in mesophyll cells of wild type and *cnl1* at different temperatures. All the cells were from the fully emerged third leaves of wild type and *cnl1* seedlings at the three-leaf stage. Bars = 2 μm (in cell view) and 1 μm (in enlarged view). H to L, Chlorophyll contents (H), greening speed (I–K), and *OsABCI7* expression (L) of etiolated wild-type and *cnl1* seedlings during the greening process. Seven-day-old etiolated seedlings were exposed to light (250 μmol m^{-2} s^{-1}) for 12 h. Bars = 2 cm. Data are means ± SD ($n = 3$). Different letters indicate significant differences by one-way ANOVA and Duncan's test ($P < 0.05$).

synthase (Hartings et al., 2017). Upon the low photosynthetic capacity in *cnl1* (Supplemental Fig. S1, D–G; Supplemental Table S2), the accumulation of major components of thylakoid membrane protein complexes in wild type and *cnl1* were determined by immunoblot to test whether thylakoid membrane complexes were impaired in *cnl1*. We tested the core subunits of PSII and PSI complexes (plastid encoded, PsaA/B and PsbA/D), nucleus-encoded light-harvesting antenna of PSI (LHCI) chlorophyll *a*/*b*-binding proteins Lhca1 to Lhca4, and nucleus-encoded LHCII type II chlorophyll *a*/*b*-binding protein Lhcb2. A pronounced reduction was observed for the levels of all these subunits except for PsaB, Lhca2, and PsbA (Fig. 6A). Additionally, the plastome-encoded NAD(P)H dehydrogenase subunit5 (NdhF) and NAD(P)H-quinone oxidoreductase subunit H (NdhH), as well as nucleus-encoded plastocyanin, β-subunit (AtpB), and epsilon-subunit (AtpE) of ATP synthase, showed notably decreased levels in *cnl1* compared with wild type (Fig. 6A). The observed reduction of almost all examined photosynthetic proteins in *cnl1* might be caused by a generally impaired rate of chloroplast protein synthesis in the mutant. Besides the thylakoid membrane proteins, soluble chloroplast proteins also should be affected by this defect. Hence, we further performed polyacrylamide SDS-PAGE to

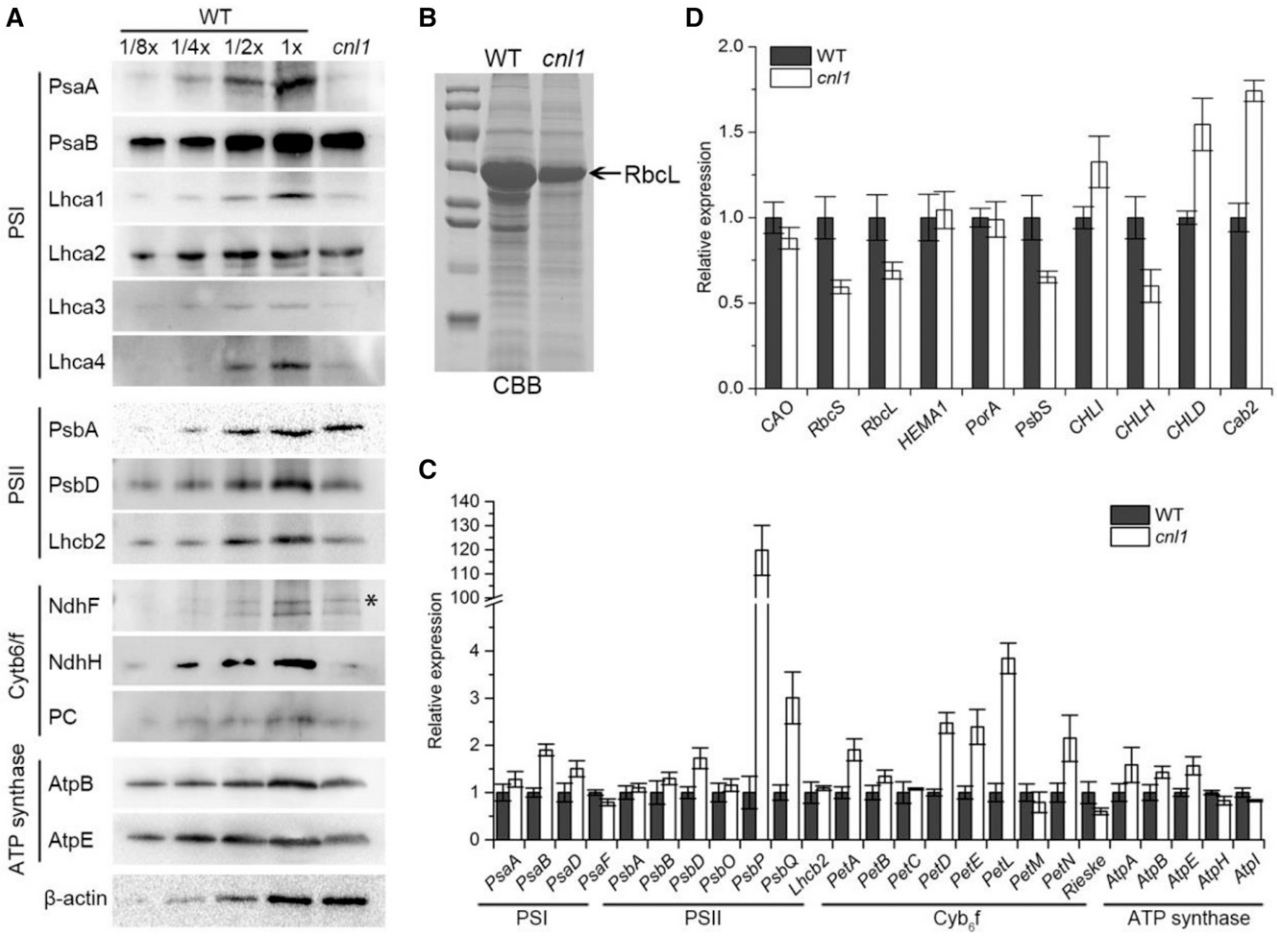

Figure 6. Levels of thylakoid membrane proteins and expression of photosynthetic genes. A, Levels of thylakoid membrane proteins detected in total proteins from flag leaves of wild type (WT) and *cnl1* at the heading stage. The wild-type dilution series contained 30 μg of proteins (1×) or the indicated dilutions, and the *cnl1* contained 30 μg proteins. Antibodies used for detection are indicated on the left; the asterisk indicates an unspecific signal detected by the NdhF antibody. B, Total proteins of flag leaves from wild type and *cnl1* mutant separated by SDS-PAGE and indicated by Coomassie Brilliant Blue (CBB) staining. C, Levels of plastid- and nucleus-encoded mRNAs related to thylakoid membrane proteins. D, Relative expression analysis of photosynthetic genes in wild-type and *cnl1*. Data are means ± SD (n = 3).

analyze the total proteins extracted from wild-type and *cnl1* flag leaves. As a soluble representative of total proteins, the level of large subunit of Rubisco (RbcL) was much lower in *cnl1* than in the wild type (Fig. 6B). Decreased accumulation of the abundant RbcL protein indicated that the reduction of different thylakoid membrane proteins in *cnl1* is the consequence of a generally defective synthesis rate of chloroplast proteins. Taken together, the results demonstrated that the thylakoid membrane protein complexes were impaired in *cnl1*.

We also detected the plastid- and nucleus-encoded transcripts of thylakoid membrane proteins by RT-qPCR, and 15 out of 25 thylakoid membrane protein-encoding genes were significantly up-regulated, while *PsaF*, *Rieske*, *AtpH*, and *AtpI* were significantly down-regulated in *cnl1* compared to wild type (Fig. 6C). Intriguingly, the immunoblot analysis showed that nearly all detected thylakoid membrane proteins were reduced in *cnl1*, which was not consistent with the RT-qPCR results, as most genes were upregulated. We speculated that the impaired thylakoid membrane protein accumulation was likely caused by a posttranslational defect in *cnl1.* The abnormal mRNA levels of photosynthesis-related genes might also imply a feedback mechanism upon the posttranslational down-regulation of thylakoid membrane proteins (Fig. 6D).

OsABCI7 Interacts with OsHCF222 in Chloroplasts

To determine the functional pathway of OsABCI7, we performed a yeast two-hybrid (Y2H) assay to screen for proteins that interact with OsABCI7. A total of 132 colonies were found positive by expressing the β-galactosidase (*lacZ*) reporter gene. Among 67 positive colonies sequenced, nine corresponded to rice *LOC_Os03g30092*. In the rice database (http://rice.plantbiology.msu.edu/), we found an orthologous gene of *LOC_Os03g30092* in

Arabidopsis named *HIGH CHLOROPHYLL FLUORESCENCE222* (*AtHCF222*); hence, we referred to rice *LOC_Os03g30092* as *OsHCF222*. To verify the localization of OsHCF222, GFP fused to the C terminus of OsHCF222 was transformed into rice protoplasts. Confocal microscopy showed GFP signals of OsHCF222-GFP fusion proteins colocalized both with the red autofluorescent signals of chloroplasts and mCherry-HDEL signals (Supplemental Fig. S9), revealing that OsHCF222 dually targeted to the chloroplasts and endoplasmic reticulum (ER), consistent with the previous localization of AtHCF222 (Hartings et al., 2017).

The conserved H-loop motif was deleted in ΔOsABCI7 (Fig. 7A; Supplemental Fig. S2). In yeast (*Saccharomyces cerevisiae*) cells and a bimolecular fluorescence complementation (BiFC) assay, we observed the interaction between OsABCI7 and OsHCF222, but no interaction between ΔOsABCI7 and OsHCF222 (Fig. 7, B and D; Supplemental Fig. S10). We therefore speculated that the H-loop motif of OsABCI7 was required for the interaction. Using Y2H and BiFC assay, we also examined the interaction between OsABCI7 with/without H-loop motif and OsHCF222. The results exhibited that both OsABCI7 (+H-loop) and OsABCI7 (−H-loop) could not interact with OsHCF222 (Fig. 7, B and D; Supplemental Fig. S10). These suggested that the C terminus of OsABCI7 was essential for the interaction between OsABCI7 and OsHCF222. Additionally, this interaction was furtherly confirmed by coimmunoprecipitation (co-IP) and BiFC assay in vivo, indicating that OsABCI7 interacts with OsHCF222 in rice chloroplasts and *Nicotiana benthamiana* cells (Fig. 7, C and D; Supplemental Fig. S10). All these demonstrated the interactions of OsABCI7 and OsHCF222 in vivo and vitro.

OsHCF222 Is Required for Biogenesis of the Thylakoid Membrane

To confirm whether both *OsABCI7* and *OsHCF222* are essential for chloroplast development, we used CRISPR/Cas9 editing to generate *Cr-OsABCI7* and

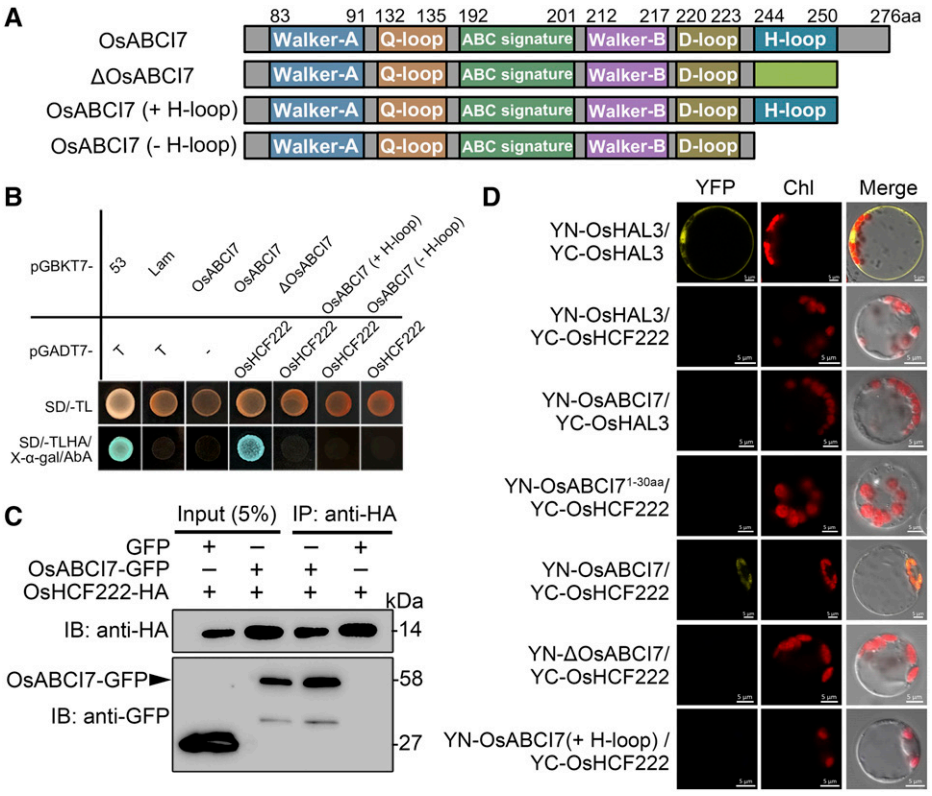

Figure 7. Interaction of OsABCI7 and OsHCF222. A, Diagrams of the wild-type OsABCI7, mutant OsABCI7 (ΔOsABCI7), OsABCI7 with H-loop motif (OsABCI7 [+H-loop]), and OsABCI7 without H-loop motif (OsABCI7 [−H-loop]). The number of amino acids is indicated at the top. B, Y2H assay for the interaction of OsABCI7 and OsHCF222. The pGBKT7-53 and pGADT7-T pair is the positive control, the pGBKT7-Lam and pGADT7-T pair is the negative control, and the pGBKT7-OsABCI7 and pGADT7 pair is the self-activation test. SD/−TL, Synthetic dropout medium without Trp and Leu; SD/−TLHA, synthetic dropout medium without Trp, Leu, His, and Adenosine; X-α-gal, 5-bromo-4-chloro-3-indoxyl-α-D-galactopyranoside; AbA, aureobasidin A. C, Co-IP assay confirmation of OsABCI7 and OsHCF222 interaction. D, BiFC assay for OsABCI7 and OsHCF222 interaction in rice protoplasts. YN-OsHAL3/YC-OsHAL3 is the positive control, YN-OsHAL3/YC-OsHCF222 and YN-ABCI7/YC-OsHAL3 are the negative controls, YN-OsABCI7^{1-30aa}/YC-OsHCF222 is a negative control to ensure that the YFP signals of YN-OsABCI7/YC-OsHCF222 are caused by the interaction between OsABCI7 and OsHCF222 instead of the chloroplast colocalization of OsABCI7 and OsHCF222. Bars = 5 μm.

Cr-OsHCF222 mutants in the cultivar Kitaake background and identified 13 *Cr-OsABCI7* and 18 *Cr-OsHCF222* knockout plants (Fig. 8, A and B). Expectedly, all *Cr-OsABCI7* knockout plants showed similar phenotypes to *cnl1* with degraded chlorophyll contents (Fig. 8, C and E; Supplemental Fig. S11), while all *Cr-OsHCF222* knockout plants exhibited severe growth retardation and much paler leaf color compared with Kitaake, and, strikingly, homozygous *Cr-OsHCF222* plants were lethal approximately 12 d after germination under conditions of soil cultivation (Fig. 8, D and F). Thus, all progenies of *Cr-OsHCF222* homozygous plants were obtained from *Cr-OsHCF222* heterozygous plants. Among 16 and 12 T_1 plants randomly chosen from two independent heterozygous *Cr-OsHCF222* lines, four and three homozygous plants were found, respectively, showing a mendelian 3:1 (wild type:mutant) ratio that indicated a single gene recessive nature of *OsHCF222*. On Suc-supplemented one-half strength Murashige and Skoog (MS) culture medium, the growth of *Cr-OsHCF222* plants was slightly retarded and the leaves were paler than those of Kitaake, whereas on Suc-free one-half strength MS medium, the *Cr-OsHCF222* plants showed more severe phenotypes than in Suc-supplemented one-half strength MS medium (Supplemental Fig. S12A). These indicated that the CRISPR/Cas9-mediated mutations of *OsHCF222* resulted in nonautotrophic seedling-lethal mutants.

The levels of thylakoid proteins in the representative *Cr-OsABCI7-2* and *Cr-OsHCF222-1* lines were compared by immunoblot analysis. In both CRISPR/Cas9 mutants, the levels of Lhcb2, Lhca3, and Lhca4 were similar to those of Kitaake, while pronounced protein reductions were found for Lhca1, Lhca2, NdhF, and AtpB in *Cr-OsHCF222-1* compared with Kitaake and *Cr-OsABCI7-2* (Fig. 8G). In contrast, PsbD and PsaB were highly accumulated in *Cr-OsABCI7-2* and *Cr-OsHCF222-1*, respectively (Fig. 8G). Compared to Kitaake, the expression of photosynthesis-related genes varied in *Cr-OsABCI7-2* but were all downregulated in *Cr-OsHCF222-1* (Supplemental Fig. S12B). Moreover, we also analyzed the expression levels of 25 thylakoid membrane genes in both mutants, and 22 genes except *PsaF*, *Lhcb2*, and *Rieske* were up-regulated in *Cr-OsABCI7-2* compared with Kitaake, and a similar upregulated expression pattern was detected in *Cr-OsHCF222-1* compared with Kitaake (Fig. 8H). This suggested that the higher transcriptional levels of thylakoid membrane genes in *Cr-OsABCI7-2* and *Cr-OsHCF222-1* did not contribute to the synthesis of thylakoid proteins. Considering that OsABCI7/OsHCF222 interaction occurs in chloroplasts, the main ROS-generating organelle, we measured the H_2O_2 contents and found both *Cr-OsABCI7-2* and *Cr-OsHCF222-1* had significantly increased H_2O_2 levels compared with Kitaake (Fig. 8, I and J).

Exogenous Antioxidants Alleviate the *cnl1* Phenotype

Considering the significant reduction of ROS levels in *OsABCI7* overexpression plants and significant accumulation in *Cr-OsHCF222* knockout plants (Fig. 2, G, H, and J), we hypothesized that OsABCI7 may interact with OsHCF222 to regulate the balance of ROS production and scavenging in chloroplasts. To demonstrate this, *cnl1* seedlings were treated with the exogenous antioxidants dimethythiourea (DMTU) and AsA (Asada, 2006; Wang et al., 2018). Under normal hydroponic conditions, *cnl1* exhibited chlorophyll degradation and H_2O_2 accumulation compared to wild type (Supplemental Fig. S13), while the *cnl1* seedlings treated with 1 mM exogenous AsA displayed an eased yellowish phenotype with significantly alleviated chlorophyll degradation (Fig. 9, A and B). We then measured the contents of H_2O_2 and O_2^- in *cnl1* under different antioxidant treatments. Higher levels of H_2O_2 and O_2^- were both detected in untreated *cnl1* seedlings compared with *cnl1* seedlings treated with 1 mM AsA (Fig. 9, C and D). As for DMTU treatment, only O_2^- but not H_2O_2 quenching was observed in treated *cnl1* seedlings (Fig. 9). Upon these results, we inferred that excessive ROS was responsible for the *cnl1* phenotype, and the exogenous AsA alleviated the yellowish phenotype of *cnl1* by relieving the ROS stress.

DISCUSSION

OsABCI7 Functions in Chloroplast Development but Its Function May Differ between Monocots and Dicots

Many leaf pigmentation mutants are usually associated with chloroplast development in rice (Wang et al., 2016; Lv et al., 2017; Sun et al., 2017; Liu et al., 2018; Cui et al., 2019). In this study, we isolated the constitutively expressed *OsABCI7*, which encodes a chloroplast-localized ABC transporter protein (Fig. 4). Due to the mutation of *OsABCI7*, *cnl1* plants mainly showed chlorotic and necrotic leaves with chloroplast structure disintegration, chlorophyll degradation, and photosynthesis impairment, finally leading to the deteriorated yield performance (Fig. 1, A–I; Supplemental Fig. S1). The chloroplast development of temperature-sensitive mutants, like *tsv*, *wsl5*, and *dua1*, is easily hindered by low temperatures in rice (Sun et al., 2017; Liu et al., 2018; Cui et al., 2019). For *cnl1*, we also observed yellowish leaves with significantly decreased chlorophyll levels and degradation of chloroplast ultrastructure at 20°C and altered mRNA levels of *OsABCI7* in response to the low-temperature stress (Fig. 5, A–G; Supplemental Fig. S8). Unlike most temperature-sensitive rice mutants, Δ*OsABCI7* leads to disabled light-dependent chlorophyll synthesis in *cnl1* during the greening process of etiolated seedlings (Fig. 5, I–K). Taken together, we conclude that OsABCI7 plays a crucial role in chloroplast biogenesis, especially under low-temperature stress and in the greening process.

The homolog of rice OsABCI7, Arabidopsis AtABCI11 (AtNAP14), participates in the regulation of chloroplast metal homeostasis and attaches to the inner envelope

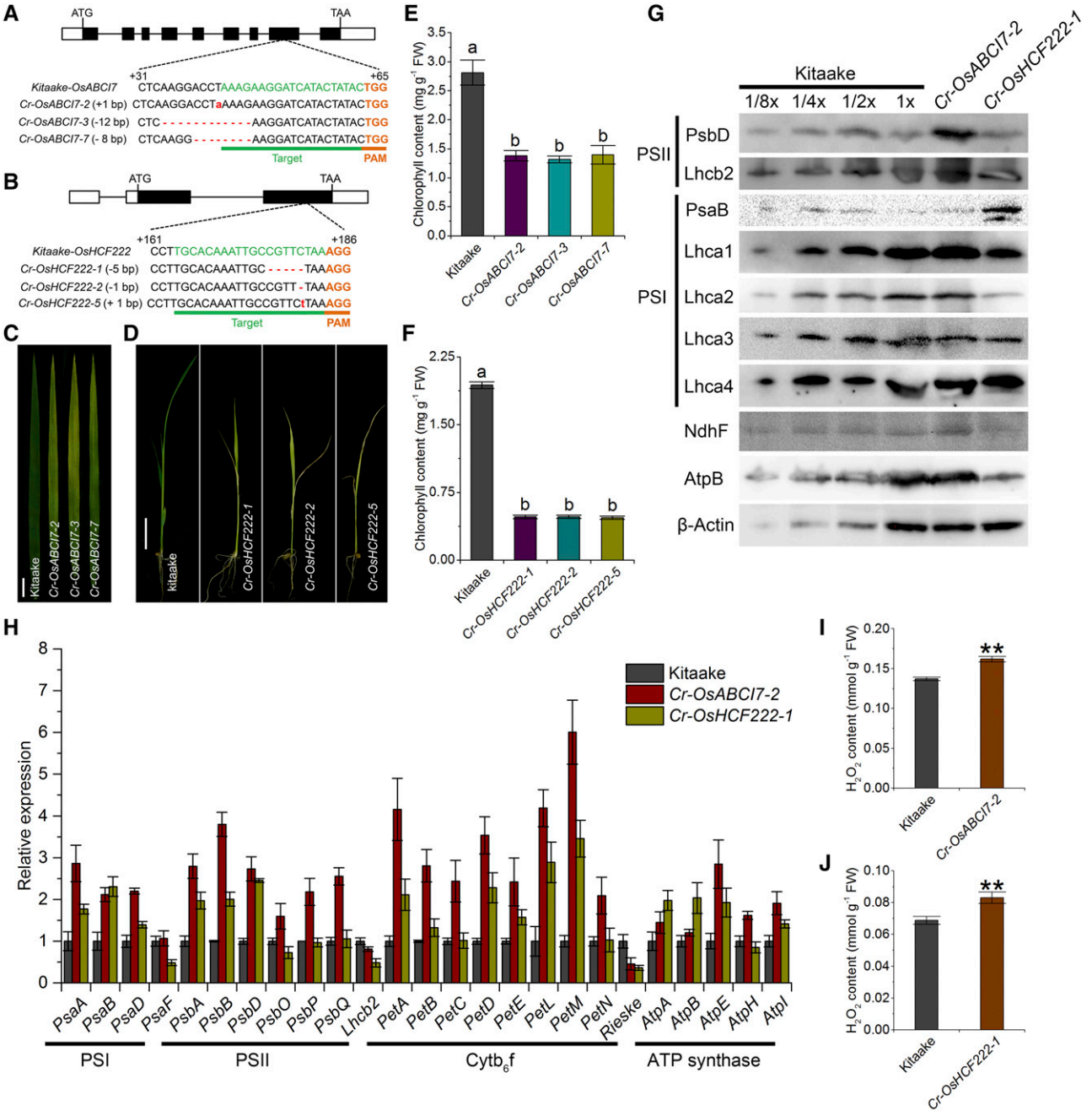

Figure 8. Characterization of CRISPR/Cas9-edited *OsABCI7* and *OsHCF222* mutations in the Kitaake background. A and B, CRISPR/Cas9-mediated mutations at the target sites of *OsABCI7* and *OsHCF222* in representative knockout lines. The sgRNA target sequence is underlined in green, and the PAM motif is indicated in orange. C, Phenotypes of flag leaves in Kitaake and *Cr-OsABCI7* knockout lines at 60 d after transplanting. D, Seedlings of T1 *Cr-OsHCF222* knockout lines at 12 d after germination. Bars = 2 cm. E and F, Chlorophyll contents of *Cr-OsABCI7* and *Cr-OsHCF222* knockout lines in C and D. Different letters indicate significant differences by one-way ANOVA and Duncan's test ($P < 0.05$). Data are means ± SD ($n = 3$). G, Levels of thylakoid membrane proteins tested in total proteins extracted from Kitaake, *Cr-OsABCI7*, and *Cr-OsHCF222* knockout lines at 8 d after germination. H, Detection of mRNA levels of plastid- and nucleus-encoded genes related to thylakoid membrane proteins in *Cr-OsABCI7-2* and *Cr-OsHCF222-1* lines at 8 DAG. I and J, Measurements of H_2O_2 contents in *Cr-OsABCI7-2* and *Cr-OsHCF222-1* at 8 DAG. Data are means ± SD ($n = 3$). Asterisks indicate significant difference by Student's *t* test (**$P < 0.01$). FW, Fresh weight.

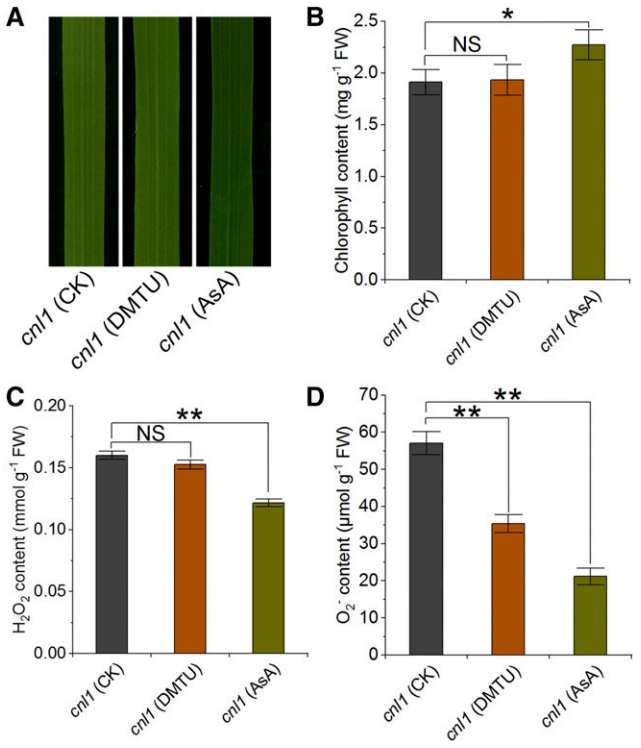

Figure 9. Responses of *cnl1* to exogenous antioxidant treatment. A, Phenotypes of fully expanded top-second leaves of *cnl1* under 1 mM DMTU and 1 mM AsA treatments. *cnl1* was hydroponically cultured for 4 d after germination and then treated with 1 mM DMTU or 1 mM AsA for 8 d. CK, Control. B to D, Chlorophyll (B), H_2O_2 (C), and O_2^- contents (D) of *cnl1* in A. Data are means ± SD ($n = 3$). Asterisks indicate significant difference by Student's *t* test (*$P < 0.05$ and **$P < 0.01$). NS, No significance.

membrane of the chloroplast; compared to the wild type (Col-0), metal elemental contents including iron (Fe), zinc (Zn), molybdenum (Mo), and copper (Cu) are higher, while manganese (Mn) is lower in *Atabci11* mutant shoot tissues, whereas Fe and Zn contents in *Atabci11* were lower than those of Col-0 in root tissues (Shimoni-Shor et al., 2010; Voith von Voithenberg et al., 2019). Hence, we determined the contents of metal elements, including magnesium (Mg), potassium (K), Fe, Cu, and Zn in the shoot and root tissues of wild type and *cnl1*. Inconsistent with the metal distribution of *Atabci11* mutants, only significant differences in Mn (1.2-fold in shoot and 2.2-fold in root) and Cu (0.8-fold in shoot and root) were detected (Supplemental Fig. S14). Mn is integral to photosynthetic electron transport, redox processes, and ROS scavenging in plants, while excessive Mn is toxic to the photosynthetic apparatus and inhibits chloroplast protein and chlorophyll synthesis (Millaleo et al., 2013; Eisenhut et al., 2018). Cu is an important minor element found in chloroplasts as a cofactor with Cu/Zn-SOD, and Cu/Zn-SOD contributes to the reduction of oxidative stress (Bowler et al., 1994; Cohu et al., 2009). The observed Mn overload and lower Cu concentration in *cnl1* may explain the chlorotic and necrotic leaf phenotypes, which are likely due to the increased ROS stress generated by the overaccumulation of Mn and decreased levels of Cu/Zn-SOD. As a transporter, OsABCI7 plays an important role in regulating chloroplast metal homeostasis (Supplemental Fig. S14). Based on this, we proposed that OsABCI7 could be a component of the chloroplast transporter complex. In addition, unlike the chloroplast inner envelope membrane-localized AtABCI11, OsABCI7 targets to the thylakoid membrane in chloroplasts (Fig. 4B). Considering the pea (*Pisum sativum*) samples used for the in vivo localization detection of AtABCI11 (Voith von Voithenberg et al., 2019), further studies need to be conducted in Arabidopsis to confirm the true in vivo localization of AtABCI11. In conclusion, these deviations of OsABCI7 and AtABCI11 might suggest different regulatory manners between monocots and dicots.

OsABCI7 Is Required for ROS-Mediated Thylakoid Membrane Stability

During the photosynthesis process at the thylakoid membrane, O_2 molecules are reduced to O_2^- by trapping electrons derived from water in PSI, and O_2^- is disproportionated to H_2O_2, catalyzed by chloroplastic SOD (Asada, 2006). Both overaccumulated ROS and a disrupted ROS scavenging system were detected in *cnl1*, indicating the impairment of ROS homeostasis (Fig. 2, G–K). As the consequence of overaccumulation of ROS, DNA fragmentation and DNA damage repair response activation were observed in *cnl1*, which exhibited an enhanced PCD manifested by trypan blue staining, TUNEL assay, and comet assay (Fig. 3; Supplemental Figs. S6C and S7). Accumulating evidence also demonstrates that ROS and cell death usually occur together (Roy et al., 2012; Luo et al., 2013; He et al., 2018a; Qiu et al., 2019; Zafar et al., 2020).

ROS are extremely active and able to interact with many kinds of target molecules and metabolites, like DNA, proteins, lipids, pigments, and other cellular molecules, resulting in a number of destructive cell processes (Ashraf, 2009). An accurate control of steady-state H_2O_2 concentration is critical to cell homeostasis, and H_2O_2 is directly scavenged by the antioxidant AsA with the catalysis of APX in healthy chloroplasts (Zhen et al., 2011; Ni et al., 2018). Notably, endogenous ROS contents of *OsABCI7* overexpression plants were significantly lower than those of wild type, which was well explained by the higher level of APX activity in overexpression plants compared to wild type (Fig. 2, G–I). We therefore speculated that *OsABCI7* is closely associated with the APX-related ROS scavenging pathway. As a consequence of *OsABCI7* disruption, newly produced ROS could not be eliminated effectively in APX pathway, leading to overaccumulation of ROS in chloroplasts. Conversely, overaccumulated ROS directly gave rise to thylakoid membrane damage, chlorophyll breakdown, and photosynthetic protein degradation,

which may be the reason for the initiation of the *cnl1* phenotype (Figs. 1, A–D, and 6, A and B). The above hypothesis was further confirmed by the easing of the *cnl1* phenotype under the treatment of exogenous antioxidant AsA (Fig. 9). In conclusion, these findings suggested that OsABCI7 is essential for ROS-mediated thylakoid membrane stability.

OsABCI7 Interacts with OsHCF222 at the Thylakoid Membrane to Regulate ROS Homeostasis

HCF proteins are required for the formation of thylakoid membrane complexes in plants (Schult et al., 2007; Link et al., 2012; Hartings et al., 2017). The Arabidopsis *AtHCF222* encodes a small protein homologous to the zinc finger domain of *Escherichia coli* chaperone DnaJ-like protein (Hartings et al., 2017). OsHCF222 shares 59% protein identity to AtHCF222 and is also characterized by eight conserved Cys-rich (CR) domains arranged in four CxxC motif clusters (Supplemental Fig. S15). Between the Cys residues of four CxxC motifs, two Zn(II) ions are coordinated to form a topology with two C4-type zinc finger structures (Shi et al., 2005). As members of the heat shock protein family, DnaJ proteins serve as cochaperones and involve in different substrate bindings, playing important roles in multiple biotic and abiotic stress responses (Liu and Whitham, 2013; Pulido and Leister, 2018).

Our results revealed physical interaction between OsABCI7 and OsHCF222 in vitro and vivo (Fig. 7, B–D; Supplemental Fig. S10). AtHCF222 is a dually ER- and chloroplast-localized protein and has been detected in leaf whole-cell membrane fractions (Hartings et al., 2017). In this study, OsHCF222 dually localized to the ER and chloroplasts, and OsABCI7 was detected in thylakoid membrane fractions by immunoblot (Fig. 4B). Upon these findings, we speculated that OsABCI7 interacts with OsHCF222 at thylakoid membranes to regulate ROS homeostasis for maintaining thylakoid integrity. To test this assumption, CRISPR/Cas9 editing was performed to obtain the corresponding knockout mutants of *OsABCI7* and *OsHCF222*. Unlike the *Cr-OsABCI7* plants, *Cr-OsHCF222* lines displayed chlorotic leaves and seedling lethality (Fig. 8, C and D). In spite of the major differences in seedling lethality and photosynthetic protein accumulation between the two types of knockout lines, ROS overaccumulation occurred in both *Cr-OsABCI7* and *Cr-OsHCF222* mutants (Fig. 8, G, I, and J). Rice DnaJ proteins are involved in chloroplast development and H_2O_2-induced DNA damage (Yamamoto et al., 2005; Zhu et al., 2015). Thus, we conclude that both OsABCI7 and OsHCF222 are essential for the thylakoid membrane development, and the OsABCI7/OsHCF222 complex plays a vital role in ROS homeostasis regulation at thylakoids. This explained that thylakoid degradation of *cnl1* was closely associated with the disruption of OsABCI7/OsHCF222 complex formation in *cnl1* (Fig. 7, A and B).

In summary, our data support the idea that OsABCI7 interacts with OsHCF222 to form a complex functioning at the thylakoid membranes in chloroplasts. We propose that the interaction is crucial to maintain thylakoid stability by regulating ROS homeostasis in chloroplasts. In *cnl1*, the disrupted interaction causes a rapid ROS burst, resulting in thylakoid instability, chloroplast breakdown, and cell death, which might in turn reinforce ROS accumulation but in a controllable manner, as *cnl1* itself and the knockout lines are viable. On the other hand, *OsHCF222* knockout lines are unviable, probably indicating that OsHCF222 is not only required for thylakoid stability but also for thylakoid membrane complex formation, as demonstrated in Arabidopsis (Schult et al., 2007; Link et al., 2012; Hartings et al., 2017).

MATERIALS AND METHODS

Plant Materials and Growth Conditions

The *cnl1* mutant was obtained from an ethyl methylsulfonate-induced indica rice (*Oryza sativa*) Zhongjian100 (wild type) mutant bank. *cnl1* mutants were crossed to the japonica rice 'ReYan 1,' 'ORO,' and wild type, respectively. All the parents, F1 plants, and F2 individuals were grown in the paddy field at Zhejiang province for genetic analysis and/or gene mapping. For the exogenous antioxidant treatments, plants were hydroponically cultured with Yoshida rice nutrient salt mixture (Coolaber, NSP1040) after germination in a growth chamber at 30°C, 14 h light/26°C, 10 h dark cycle. The *cnl1* seedlings without antioxidant treatment were used as the control (CK). The nutrient solution containing either 1mM DMTU or 1 mM AsA was used for antioxidant treatments.

Chlorophyll Measurement, TEM, and Paraffin Sectioning

Chlorophyll content was determined by measuring the A_{652} using a SpectraMax i3x multi-mode microplate reader (Molecular Devices) as described previously (Kim et al., 2006). Leaves were collected to perform TEM according to a previous report (He et al., 2018a). The third internodes of the main stem from wild type and *cnl1* at the mature stage were used for paraffin sections as described previously (He et al., 2017).

MDA, ROS Content, and Antioxidant Activity Measurement

The contents of MDA, as well as the activities of ROS scavenging enzymes, including peroxidase, SOD, and CAT, were determined using the kits (A003-1-2, A084-1-1, A001-1-1, and A007-1-1) following the manufacturer's instructions (Nanjing Jiancheng Bioengineering Institute). H_2O_2 content was determined using the H_2O_2 assay kit (Nanjing Jiancheng Bioengineering Institute), and the level of O_2^- was quantified using a kit (R30343) following the manufacturer's instructions (Shanghai Yuanye Bio-Technology).

Map-Based Cloning

The mutant F2 individuals from the *cnl1*/cv ReYan 1 cross were selected for mapping the *OsABCI7* locus. Bulked segregant analysis was adopted to rapidly locate the mutation as follows: equal amounts of leaf blades from each of 10 wild-type plants, and 10 *cnl1* plants were sampled for DNA extraction to form a wild-type DNA pool and a mutant DNA pool, respectively. The parents and the two DNA pools were subjected to preliminary linkage analysis of the mutation by genotyping 362 polymorphic simple sequence repeat markers covering 12 chromosomes. Subsequently, 755 *cnl1* individual plants from the F2 population were genotyped to determine the physical location of *OsABCI7*. Primers used for mapping are listed in Supplemental Table S3.

RNA Extraction and RT-qPCR

Total RNA was extracted using a NucleoZOL reagent kit (MACHEREY-NAGEL) according to the manufacturer's instructions. One microgram total RNA was reverse-transcribed using the ReverTra Ace RT-qPCR RT master mix with genomic DNA remover kit (Toyobo). Rice *Ubiquitin* (*LOC_Os03g13170*) was used as an internal control. Primers used for RT-qPCR are listed in Supplemental Table S3.

Generation of Transgenic Plants

For the complementation of *cnl1*, the wild-type allele containing the 1788-bp promoter region, entire genomic DNA region (3384 bp), and 711 bp downstream of *OsABCI7* was cloned into the vector pCAMBIA1300. To generate the overexpression lines, the 831-bp CDS of *OsABCI7* was cloned into the vector pCAMBIA1300-UBI under the control of the maize (*Zea mays*) *Ubiquitin1* promoter. For the promoter activity assay of *OsABCI7*, the *OsABCI7* promoter was inserted into the vector pCAMBIA1381Z containing the *GUS* gene. The CRISPR/Cas9 constructs for *OsABCI7* and *OsHCF222* were generated according to a previous report (Ma et al., 2015). The genetic transformations were conducted using rice embryogenic calli through *Agrobacterium tumefaciens*-mediated transformation (Hiei and Komari, 2008). Primers used for vector constructions are listed in Supplemental Table S3.

Subcellular Localization and Chloroplast-Localized Signal Peptide Analysis

To determine the subcellular localization of OsABCI7 and OsHCF222, the CDS of *OsABCI7* and *OsHCF222* amplified from wild type were fused to the N terminus of *GFP* in the pAN580 (GFP) vector, respectively. To determine the chloroplast-localized signal peptide region, different truncated CDS of *OsABCI7* were also fused to the N terminus of *GFP* in the pAN580 vector. All these constructs were separately introduced into rice protoplasts for transient expression, and the GFP fluorescence signals were detected using a Zeiss lsm710 confocal laser scanning microscope (Carl Zeiss).

$OsABCI7_{Pro}$::*GUS* Staining Assay

Different tissues from *OsABCI7*-promoter-*GUS* transgenic plants were collected at different growth stages and stained using a *GUS* staining kit (Coolaber, SL7160), following the manufacturer's instructions. Images were photographed using a stereomicroscope (Leica MC120 HD).

Comet Assay

The alkaline comet assay was performed according to Wang and Liu (2006) using the Comet assay kit from Trevigen. The SYBR green I nucleic acid gel stain (S9430) purchased from Sigma-Aldrich was used for staining. Thirty to 70 comets were counted in each slide, and DNA damage was classified into four degrees as previously reported (Yuan et al., 2010).

Y2H Assay

The cDNA library constructed from Nipponbare embryogenic calli and the screening kit (Clontech) were used for Y2H assays. All protocols were carried out strictly according to the manufacturer's user manual. The full CDS of *OsABCI7* and *OsHCF222* amplified from wild-type cDNA and the mutant full CDS amplified from *cnl1* were cloned into the pGBKT7 or pGADT7 vector, respectively. The truncated CDS of *OsABCI7* with/without specific domains from the wild type were also cloned into the pGBKT7 vector. The yeast (*Saccharomyces cerevisiae*) strain Y2HGold was used in the Y2H assay. Primers used are listed in Supplemental Table S3.

BiFC Assay

For BiFC assays, the entire CDS of *OsABCI7*, 90 bp of the N-terminal *OsABCI7* CDS, the CDS of Δ*OsABCI7*, and *OsABCI7* with the H-loop motif were cloned into the 1300-YN vector. The entire CDS of *OsHCF222* was cloned into the 2300-YC vector. The new constructs were electroporated into *A. tumefaciens* strain GV3101 for transient expression in *Nicotiana benthamiana* leaves and were also introduced into rice protoplasts for transient expression. The YFP fluorescent signals in the *N. benthamiana* leaves were detected ~48 h after transfection, and the YFP signals in rice protoplasts were observed about 36 h after expression.

Protein Extraction and Immunoblot Analysis

Total proteins were extracted as previously described (He et al., 2018b) and quantified into the same concentration using the BCA protein assay kit (Coolaber, SK1070). For intact chloroplast isolation, 1 g fresh leaf tissue from *OsABCI7* overexpression seedlings was collected for chloroplast isolation using the chloroplast isolation kit (BestBio, BB-3622) following the manufacturer's instructions. To directly isolate the thylakoid membranes, 1 g fresh leaf tissue was homogenized on ice with 5 mL extraction buffer (0.4 M Suc, 10 mM NaCl, 2 mM $MgCl_2$, and 50 mM HEPES), then filtered through two layers of 40 μM nylon membrane and centrifuged for 10 min at 4°C, 5000*g*. After discarding the supernatant, the sediment was rinsed with 1 mL extraction buffer, then centrifuged for 10 min at 4°C, 5000*g*, repeating this step twice. Finally, the sediment was resuspended with the extraction buffer and stored at −80°C. Antibodies used for immunoblot analysis of thylakoid membrane proteins were purchased from Agrisera, and the products and catalog numbers are as follows: anti-PsaA (AS06172), anti-PsaB (AS10695), anti-Lhca1 (AS01005), anti-Lhca2 (AS01006), anti-Lhca3 (AS01007), anti-Lhca4 (AS01008), anti-PsbA (AS132669), anti-PsbD (AS06146), anti-Lhcb1 (AS01004), anti-Lhcb2 (AS01003), anti-NdhH (AS132712), anti-NdhF (AS132711), anti-plastocyanin (AS06141), anti-AtpB (AS05085), and anti-AtpE (AS101586). The protein levels were detected using a super ECL western blotting substrate (Coolaber, SL1350).

Co-IP Assay

For the Co-IP assay, the full CDS of *OsABCI7* was cloned into pYBA1132-GFP, and the CDS of *OsHCF222* was cloned into pYBA1132-HA, respectively. The constructs were transiently expressed in *N. benthamiana* leaves via *A. tumefaciens*-mediated transfection. About 60 h after transfection, fresh *N. benthamiana* leaves were harvested for total protein extraction using the buffer (0.4 mM Tris-HCl, pH 7.5, 5 mM NaCl, 6.25 μM $MgCl_2$, 10 μM EDTA, and 1% Triton X-100) with proteinase inhibitor cocktail (Roche, 04693159001). The supernatant of total proteins was collected after centrifugation at 12,000*g* for 20 min at 4°C. The Pierce HA-tag magnetic IP/co-IP kit (88838X) was used for the Co-IP assay following the manufacturer's manual. Anti-GFP (Abmart, M200045) and anti-HA (CWBIO, CW0092M) antibodies were used for detection in immunoblot analysis.

Accession Numbers

Sequence data from this article for the cDNA and genomic DNA of *OsABCI7* and *OsHCF222* can be found in the GenBank/EMBL/Gramene data libraries under accession numbers *LOC_Os11g29850* and *LOC_Os03g30092*, respectively.

Supplemental Data

The following supplemental materials are available.

Supplemental Figure S1. Phenotypic and photosynthetic analysis of wild type and *cnl1*.

Supplemental Figure S2. CDS of *OsABCI7* and amino acid sequence of OsABCI7.

Supplemental Figure S3. Mutation analysis of *OsABCI7*.

Supplemental Figure S4. Overexpression of *OsABCI7* and analysis of *OsABCI7*-RNA-interference lines.

Supplemental Figure S5. Soluble protein contents and SOD activities in wild type, *cnl1*, complementary, and overexpression lines.

Supplemental Figure S6. Chlorophyll contents and histochemical analysis.

Supplemental Figure S7. TUNEL assay of wild type and *cnl1*.

Supplemental Figure S8. Chlorophyll contents and *OsABCI7* expression analysis.

Supplemental Figure S9. Subcellular localization of OsHCF222.

Supplemental Figure S10. BiFC for the interaction of OsABCI7 and OsHCF222 in *N. benthamiana*.

Supplemental Figure S11. Knockout analysis of *OsABCI7* by CRISPR/Cas9 technology.

Supplemental Figure S12. Phenotypes of *OsHCF222* knockout line and expression of photosynthesis-related genes in *OsABCI7* and *OsHCF222* knockout lines.

Supplemental Figure S13. Chlorophyll and H_2O_2 contents in wild-type and *cnl1* seedlings.

Supplemental Figure S14. Levels of metal elements in shoots and roots of wild type and *cnl1*.

Supplemental Figure S15. Alignment of HCF222 orthologs from different plant species.

Supplemental Table S1. List of ORFs in the 116-kb target region.

Supplemental Table S2. Chlorophyll fluorescence parameters measured in flag leaves of wild-type, *cnl1*, complementary, and overexpression lines.

Supplemental Table S3. Primers used in this study.

Received April 30, 2020; accepted June 23, 2020; published July 13, 2020.

LITERATURE CITED

Ahmad P, Jaleel CA, Salem MA, Nabi G, Sharma S (2010) Roles of enzymatic and nonenzymatic antioxidants in plants during abiotic stress. Crit Rev Biotechnol **30:** 161–175

Asada K (1992) Ascorbate peroxidase—a hydrogen peroxide-scavenging enzyme in plants. Physiol Plant **85:** 235–241

Asada K (2006) Production and scavenging of reactive oxygen species in chloroplasts and their functions. Plant Physiol **141:** 391–396

Asada K, Kiso K, Yoshikawa K (1974) Univalent reduction of molecular oxygen by spinach chloroplasts on illumination. J Biol Chem **249:** 2175–2181

Ashraf M (2009) Biotechnological approach of improving plant salt tolerance using antioxidants as markers. Biotechnol Adv **27:** 84–93

Bowler C, Van Camp W, Van Montagu M, Inze D, Asada K (1994) Superoxide dismutase in plants. Crit Rev Plant Sci **13:** 199–218

Buchanan-Wollaston V, Earl S, Harrison E, Mathas E, Navabpour S, Page T, Pink D (2003) The molecular analysis of leaf senescence—a genomics approach. Plant Biotechnol J **1:** 3–22

Cohu CM, Abdel-Ghany SE, Gogolin Reynolds KA, Onofrio AM, Bodecker JR, Kimbrel JA, Niyogi KK, Pilon M (2009) Copper delivery by the copper chaperone for chloroplast and cytosolic copper/zinc-superoxide dismutases: Egulation and unexpected phenotypes in an *Arabidopsis* mutant. Mol Plant **2:** 1336–1350

Cui X, Wang Y, Wu J, Han X, Gu X, Lu T, Zhang Z (2019) The RNA editing factor DUA1 is crucial to chloroplast development at low temperature in rice. New Phytol **221:** 834–849

Culligan KM, Robertson CE, Foreman J, Doerner P, Britt AB (2006) ATR and ATM play both distinct and additive roles in response to ionizing radiation. Plant J **48:** 947–961

Durrant WE, Wang S, Dong X (2007) *Arabidopsis SNI1* and *RAD51D* regulate both gene transcription and DNA recombination during the defense response. Proc Natl Acad Sci USA **104:** 4223–4227

Eisenhut M, Hoecker N, Schmidt SB, Basgaran RM, Flachbart S, Jahns P, Eser T, Geimer S, Husted S, Weber APM, et al (2018) The plastid envelope CHLOROPLAST MANGANESE TRANSPORTER1 is essential for manganese homeostasis in *Arabidopsis*. Mol Plant **11:** 955–969

Garcia O, Bouige P, Forestier C, Dassa E (2004) Inventory and comparative analysis of rice and Arabidopsis ATP-binding cassette (ABC) systems. J Mol Biol **343:** 249–265

Garroum I, Bidzinski P, Daraspe J, Mucciolo A, Humbel BM, Morel JB, Nawrath C (2016) Cuticular defects in *Oryza sativa* ATP-binding cassette transporter G31 mutant plants cause dwarfism, elevated defense responses and pathogen resistance. Plant Cell Physiol **57:** 1179–1188

Gill SS, Tuteja N (2010) Reactive oxygen species and antioxidant machinery in abiotic stress tolerance in crop plants. Plant Physiol Biochem **48:** 909–930

Hartings S, Paradies S, Karnuth B, Eisfeld S, Mehsing J, Wolff C, Levey T, Westhoff P, Meierhoff K (2017) The DnaJ-like zinc-finger protein HCF222 is required for thylakoid membrane biogenesis in plants. Plant Physiol **174:** 1807–1824

He Y, Li L, Zhang Z, Wu JL (2018a) Identification and comparative analysis of premature senescence leaf mutants in rice (*Oryza sativa* L.). Int J Mol Sci **19:** 140

He Y, Shi YF, Zhang XB, Wang HM, Xu X, Wu JL (2017) Identification of a gravitropism-deficient mutant in rice. Rice Sci **24:** 109–118

He Y, Zhang Z, Li L, Tang S, Wu JL (2018b) Genetic and physiobiochemical characterization of a novel premature senescence leaf mutant in rice (*Oryza sativa* L.). Int J Mol Sci **19:** 2339

Hiei Y, Komari T (2008) *Agrobacterium*-mediated transformation of rice using immature embryos or calli induced from mature seed. Nat Protoc **3:** 824–834

Huang CF, Yamaji N, Mitani N, Yano M, Nagamura Y, Ma JF (2009) A bacterial-type ABC transporter is involved in aluminum tolerance in rice. Plant Cell **21:** 655–667

Huang QN, Shi YF, Zhang XB, Song LX, Feng BH, Wang HM, Xu X, Li XH, Guo D, Wu JL (2016) Single base substitution in *OsCDC48* is responsible for premature senescence and death phenotype in rice. J Integr Plant Biol **58:** 12–28

Kim HJ, Ryu H, Hong SH, Woo HR, Lim PO, Lee IC, Sheen J, Nam HG, Hwang I (2006) Cytokinin-mediated control of leaf longevity by AHK3 through phosphorylation of ARR2 in *Arabidopsis*. Proc Natl Acad Sci USA **103:** 814–819

Kobayashi K, Kondo M, Fukuda H, Nishimura M, Ohta H (2007) Galactolipid synthesis in chloroplast inner envelope is essential for proper thylakoid biogenesis, photosynthesis, and embryogenesis. Proc Natl Acad Sci USA **104:** 17216–17221

Link S, Engelmann K, Meierhoff K, Westhoff P (2012) The atypical short-chain dehydrogenases HCF173 and HCF244 are jointly involved in translational initiation of the *psbA* mRNA of Arabidopsis. Plant Physiol **160:** 2202–2218

Liu JZ, Whitham SA (2013) Overexpression of a soybean nuclear localized type-III DnaJ domain-containing HSP40 reveals its roles in cell death and disease resistance. Plant J **74:** 110–121

Liu X, Lan J, Huang YS, Cao PF, Zhou CL, Ren YK, He NQ, Liu SJ, Tian YL, Nguyen T, et al (2018) WSL5, a pentatricopeptide repeat protein, is essential for chloroplast biogenesis in rice under cold stress. J Exp Bot **69:** 3949–3961

Luo H, Yang A, Schulte BA, Wargovich MJ, Wang GY (2013) Resveratrol induces premature senescence in lung cancer cells via ROS-mediated DNA damage. PLoS One **8:** e60065

Lv Y, Shao G, Qiu J, Jiao G, Sheng Z, Xie L, Wu Y, Tang S, Wei X, Hu P (2017) *White Leaf and Panicle 2*, encoding a PEP-associated protein, is required for chloroplast biogenesis under heat stress in rice. J Exp Bot **68:** 5147–5160

Lyska D, Meierhoff K, Westhoff P (2013) How to build functional thylakoid membranes: From plastid transcription to protein complex assembly. Planta **237:** 413–428

Ma X, Zhang Q, Zhu Q, Liu W, Chen Y, Qiu R, Wang B, Yang Z, Li H, Lin Y, et al (2015) A robust CRISPR/Cas9 system for convenient, high-efficiency multiplex genome editing in monocot and dicot plants. Mol Plant **8:** 1274–1284

Matsuda S, Funabiki A, Furukawa K, Komori N, Koike M, Tokuji Y, Takamure I, Kato K (2012) Genome-wide analysis and expression profiling of half-size ABC protein subgroup G in rice in response to abiotic stress and phytohormone treatments. Mol Genet Genomics **287:** 819–835

Meurer J, Meierhoff K, Westhoff P (1996) Isolation of high-chlorophyll-fluorescence mutants of *Arabidopsis thaliana* and their characterisation by spectroscopy, immunoblotting and northern hybridisation. Planta **198:** 385–396

Millaleo R, Reyes-Díaz M, Alberdi M, Ivanov AG, Krol M, Hüner NP (2013) Excess manganese differentially inhibits photosystem I versus II in *Arabidopsis thaliana*. J Exp Bot **64:** 343–354

Ni Y, Liu H, Dai D, Mu X, Xu J, Shao S (2018) Chromogenic, fluorescent, and redox sensors for multichannel imaging and detection of hydrogen peroxide in living cell systems. Anal Chem **90:** 10152–10158

Pulido P, Leister D (2018) Novel DNAJ-related proteins in *Arabidopsis thaliana*. New Phytol **217:** 480–490

Qiu Z, Zhu L, He L, Chen D, Zeng D, Chen G, Hu J, Zhang G, Ren D, Dong G, et al (2019) DNA damage and reactive oxygen species cause cell death in the rice *local lesions 1* mutant under high light and high temperature. New Phytol **222:** 349–365

Roy N, Bagchi S, Raychaudhuri P (2012) Damaged DNA binding protein 2 in reactive oxygen species (ROS) regulation and premature senescence. Int J Mol Sci **13:** 11012–11026

Sathe AP, Su X, Chen Z, Chen T, Wei X, Tang S, Zhang XB, Wu JL (2019) Identification and characterization of a spotted-leaf mutant *spl40* with enhanced bacterial blight resistance in rice. Rice (N Y) **12:** 68

Schult K, Meierhoff K, Paradies S, Töller T, Wolff P, Westhoff P (2007) The nuclear-encoded factor HCF173 is involved in the initiation of translation of the *psbA* mRNA in *Arabidopsis thaliana*. Plant Cell **19:** 1329–1346

Shi YY, Tang W, Hao SF, Wang CC (2005) Contributions of cysteine residues in Zn2 to zinc fingers and thiol-disulfide oxidoreductase activities of chaperone DnaJ. Biochemistry **44:** 1683–1689

Shimoni-Shor E, Hassidim M, Yuval-Naeh N, Keren N (2010) Disruption of Nap14, a plastid-localized non-intrinsic ABC protein in *Arabidopsis thaliana* results in the over-accumulation of transition metals and in aberrant chloroplast structures. Plant Cell Environ **33:** 1029–1038

Soares C, Sousa AD, Pinto A, Azenha M, Teixeira J, Azevedo RA, Fidalgo F (2016) Effect of 24-epibrassinolide on ROS content, antioxidant system, lipid peroxidation and Ni uptake in *Solanum nigrum L.* under Ni stress. Environ Exp Bot **122:** 115–125

Song X, Wang D, Ma L, Chen Z, Li P, Cui X, Liu C, Cao S, Chu C, Tao Y, et al (2012) Rice RNA-dependent RNA polymerase 6 acts in small RNA biogenesis and spikelet development. Plant J **71:** 378–389

Speit G, Hartmann A (2006) The comet assay: a sensitive genotoxicity test for the detection of DNA damage and repair. Methods Mol Biol **314:** 275–286

Sun J, Zheng T, Yu J, Wu T, Wang X, Chen G, Tian Y, Zhang H, Wang Y, Terzaghi W, et al (2017) TSV, a putative plastidic oxidoreductase, protects rice chloroplasts from cold stress during development by interacting with plastidic thioredoxin Z. New Phytol **215:** 240–255

Voith von Voithenberg L, Park J, Stübe R, Lux C, Lee Y, Philippar K (2019) A novel prokaryote-type ECF/ABC transporter module in chloroplast metal homeostasis. Front Plant Sci **10:** 1264

Wang B, Zhang Y, Bi Z, Liu Q, Xu T, Yu N, Cao Y, Zhu A, Wu W, Zhan X, et al (2019) Impaired function of the calcium-dependent protein kinase, *OsCPK12*, leads to early senescence in rice (*Oryza sativa* L.). Front Plant Sci **10:** 52

Wang C, Liu Z (2006) *Arabidopsis* ribonucleotide reductases are critical for cell cycle progression, DNA damage repair, and plant development. Plant Cell **18:** 350–365

Wang X, Dong X, Feng Y, Liu X, Wang J, Zhang Z, Li J, Zhao Y, Shi S, Tu P (2018) H_2O_2 and NADPH oxidases involve in regulation of 2-(2-phenylethyl)chromones accumulation during salt stress in *Aquilaria sinensis* calli. Plant Sci **269:** 1–11

Wang Y, Zhang J, Shi X, Peng Y, Li P, Lin D, Dong Y, Teng S (2016) Temperature-sensitive albino gene *TCD5*, encoding a monooxygenase, affects chloroplast development at low temperatures. J Exp Bot **67:** 5187–5202

Wang Z, Hong X, Hu K, Wang Y, Wang X, Du S, Li Y, Hu D, Cheng K, An B, et al (2017) Impaired magnesium protoporphyrin IX methyltransferase (ChlM) impedes chlorophyll synthesis and plant growth in rice. Front Plant Sci **8:** 1694

Xu X, Chen Z, Shi YF, Wang HM, He Y, Shi L, Chen T, Wu JL, Zhang XB (2018) Functional inactivation of *OsGCNT* induces enhanced disease resistance to *Xanthomonas oryzae* pv. *oryzae* in rice. BMC Plant Biol **18:** 264

Yamamoto T, Mori Y, Ishibashi T, Uchiyama Y, Ueda T, Ando T, Hashimoto J, Kimura S, Sakaguchi K (2005) Interaction between proliferating cell nuclear antigen (PCNA) and a DnaJ induced by DNA damage. J Plant Res **118:** 91–97

Yoo SC, Cho SH, Sugimoto H, Li J, Kusumi K, Koh HJ, Iba K, Paek NC (2009) Rice *virescent3* and *stripe1* encoding the large and small subunits of ribonucleotide reductase are required for chloroplast biogenesis during early leaf development. Plant Physiol **150:** 388–401

Yuan Z, Luo D, Li G, Yao X, Wang H, Zeng M, Huang H, Cui X (2010) Characterization of the *AE7* gene in *Arabidopsis* suggests that normal cell proliferation is essential for leaf polarity establishment. Plant J **64:** 331–342

Zafar SA, Patil SB, Uzair M, Fang J, Zhao J, Guo T, Yuan S, Uzair M, Luo Q, Shi J, et al (2020) *DEGENERATED PANICLE AND PARTIAL STERILITY 1* (*DPS1*) encodes a cystathionine β-synthase domain containing protein required for anther cuticle and panicle development in rice. New Phytol **225:** 356–375

Zeng X, Tang R, Guo H, Ke S, Teng B, Hung YH, Xu Z, Xie XM, Hsieh TF, Zhang XQ (2017) A naturally occurring conditional albino mutant in rice caused by defects in the plastid-localized OsABCI8 transporter. Plant Mol Biol **94:** 137–148

Zhang XB, Feng BH, Wang HM, Xu X, Shi YF, He Y, Chen Z, Sathe AP, Shi L, Wu JL (2018) A substitution mutation in *OsPELOTA* confers bacterial blight resistance by activating the salicylic acid pathway. J Integr Plant Biol **60:** 160–172

Zhao G, Shi J, Liang W, Xue F, Luo Q, Zhu L, Qu G, Chen M, Schreiber L, Zhang D (2015) Two ATP binding cassette G transporters, rice ATP binding cassette G26 and ATP binding cassette G15, collaboratively regulate rice male reproduction. Plant Physiol **169:** 2064–2079

Zhen A, Bie Z, Huang Y, Liu Z, Lei B (2011) Effects of salt-tolerant rootstock grafting on ultrastructure, photosynthetic capacity, and H_2O_2-scavenging system in chloroplasts of cucumber seedlings under NaCl stress. Acta Physiol Plant **33:** 2311–2319

Zhou BB, Elledge SJ (2000) The DNA damage response: Putting checkpoints in perspective. Nature **408:** 433–439

Zhu X, Liang S, Yin J, Yuan C, Wang J, Li W, He M, Wang J, Chen W, Ma B, et al (2015) The DnaJ OsDjA7/8 is essential for chloroplast development in rice (*Oryza sativa*). Gene **574:** 11–19